JNC TN8400 2000-005

Compilation of Kinetic Data for Geochemical Calculations

January 2000

Tokai Works
Japan Nuclear Cycle Development Institute

Compilation of Kinetic Data for Geochemical Calculations

Randolph C Arthur[1], David Savage[2], Hiroshi Sasamoto[3]
Masahiro Shibata[3], Mikazu Yui[3]

Abstract

Kinetic data, including rate constants, reaction orders and activation energies, are compiled for 34 hydrolysis reactions involving feldspars, sheet silicates, zeolites, oxides, pyroxenes and amphiboles, and for similar reactions involving calcite and pyrite. The data are compatible with a rate law consistent with surface reaction control and transition-state theory, which is incorporated in the geochemical software package EQ3/6 and GWB. Kinetic data for the reactions noted above are strictly compatible with the transition-state rate law only under far-from-equilibrium conditions. It is possible that the data are conceptually consistent with this rate law under both far-from-equilibrium and near-to-equilibrium conditions, but this should be confirmed whenever possible through analysis of original experimental results.

Due to limitations in the availability of kinetic data for mineral-water reactions, and in order to simplify evaluations of geochemical models of groundwater evolution, it is convenient to assume local-equilibrium in such models whenever possible. To assess whether this assumption is reasonable, a modeling approach accounting for coupled fluid flow and water-rock interaction is described that can be used to estimate spatial and temporal scale of local equilibrium. The approach is demonstrated for conditions involving groundwater flow in fractures at JNC's Kamaishi *in-situ* tests site, and is also used to estimate the travel time necessary for oxidizing surface waters to migrate to the level of a HLW repository in crystalline rock.

The question of whether local equilibrium is a reasonable assumption must be addressed using an appropriate modeling approach. To be appropriate for conditions at the Kamaishi site using the modeling approach noted above, the fracture fill must closely approximate a porous medium, groundwater flow must be purely advective and diffusion of solutes across the fracture-host rock boundary must not occur. Moreover, the mineralogical and physical properties of the fracture must be homogeneous over a characteristic length that is greater than or equal to the equilibration length.

If these conditions are met, calculations suggest local equilibrium would be a valid assumption in groundwater evolution models applied to the Kamaishi site if:

- it applies to reactions involving calcite, stilbite (assuming its dissolution / precipitation behavior is similar to that of heulandite), laumontite, albite and prehnite, but not quartz;
- Darcy flow velocities are relatively low (e.g., less than about 0.1 m yr-1), and
- it is based on the assumption that equilibrium corresponds to an uncertainty in the saturation index of 0.0 ± 0.4

If, however, actual reaction rates in the field are lower than expected, possibly because reactive surface areas are overestimated, the modeling approach may be inappropriate because it is probably unrealistic to assume that fracture mineralogy is homogeneous over fracture lengths exceeding a few meters or tens of meters.

An analytical model of redox-front migration behavior based on the stationary-state approximation, and JNC's conceptual model of a natural events scenario involving the migration of oxidizing surface waters in fractures, suggests that oxidizing solutions could travel from the surface to the depth of a repository in crystalline rock within 400 to 50,000 years. These estimates are relatively short compared with time periods considered in safety assessments of repository performance, which suggests that time-dependent variations in the redox environment of both the near field and geosphere may need to be accounted for in these assessments. The flow velocities and concentrations of reducing minerals assumed in JNC's conceptual model may be overly conservative, however.

---

1) Monitor Scientific, LLC., Denver, Colorado, USA

2) Quintessa, Ltd., Nottingham, UK

3) Japan Nuclear Cycle Development Institute Tokai Works, Tokai-Mura, Ibaraki, Japan

地球化学計算のための速度論データの収集
（研究報告）

Randolph C Arthur[1], David Savage[2], 笹本 広[3]
柴田雅博[3], 油井三和[3]

要 旨

本報告書では，長石，層状珪酸塩，沸石，酸化物，輝石，角閃石に対する 34 種類の水和反応を対象に速度定数，反応次数，活性化エネルギーを含む速度論データを収集・整理した。また，同様に方解石と黄鉄鉱に対する速度論データも収集・整理した。これらのデータは，地球化学コードである EQ3/6 や GWB で用いられている表面反応支配・遷移状態理論に則した速度則に適合する。上述した水和反応の速度論データは，厳密には，平衡状態からかけ離れた非平衡状態における遷移状態速度則に適合するものである。これらのデータは，平衡状態からかけ離れた非平衡状態および平衡状態に近い状態における速度則にも概念的には適合するものであるが，その妥当性は，元文献の実験結果の解析を通じて可能な限り確認されるべきである。

鉱物－水反応に関する速度論データの適用性の限界を考慮し，地下水水質形成の地球化学モデルの評価を単純化する上で，可能な場合，部分平衡を仮定することは有効な方法である。部分平衡の仮定が妥当であるかどうかを評価するため，部分平衡の空間的，時間的スケールを評価するために用いられる水理および水－岩石反応を結合したモデル化手法について記述した。この様なモデル化手法は，釜石原位置試験場における割れ目中での地下水流れを含む条件に対して適用され，また，酸化性の地表水が結晶質岩における高レベル放射性廃棄物の処分深度にまで達するのに要する時間を評価するためにも用いられた。

部分平衡が妥当な仮定であるかどうかといった疑問に対しては，適切なモデル化手法をもとに検討されるべきである。上述したモデル化手法を用いて，釜石サイトでの条件に適用するためには，割れ目充填部は多孔質媒体に近似でき，地下水の流れは単なる移流のみであり，母岩マトリクス方向への拡散は生じないことになる。さらに，平衡状態に達するまでの距離と同じか，それよりも長い距離に渡って，割れ目の鉱物学的特性や物理学的特性が均一でなければならない。

もしこの様な条件下において，以下の状態であるならば，釜石サイトにおける地下水水質形成モデルにおいて部分平衡を仮定することが妥当であると推測される。

・方解石，濁沸石（その溶解・沈殿挙動が輝沸石に類似すると仮定），濁沸石，葡萄石，（石英は含まない）
・ダルシー流速は比較的小さい（たとえば，約 0.1 m yr-1）
・平衡状態に関する不確実性として，飽和指数で±0.4 を誤差として仮定する

しかしながら，反応比表面積を過剰に見込んだために見積もられる可能性として，フィールドにおける実際の反応速度が予想される速度よりも遅い場合，割れ目の充填鉱物が 2～3m から数十 m に渡って均一であることを仮定するのは恐らく非現実的であるため，この様なモデル化手法は不適当であるかもしれない。

遷移状態近似に基づく酸化還元フロントの解析モデルおよび割れ目を通じた酸化性の地表水の浸入を含む天然事象に関するシナリオの概念モデルから，400 年～50,000 年の間に酸化性の地表水が地表から結晶質岩における処分深度にまで達する可能性が示唆された。この様な評価期間は，処分場性能の安全評価において考慮される期間に比べて短く，従って，安全評価において，ニアフィールドおよび地層中での酸化還元環境の変化の時間依存性を考慮する必要があるかもしれない。但し，今回考慮した概念モデルにおいて仮定した流速や還元物質の濃度は，かなり保守的な仮定であるかもしれない。

---

1) Monitor Scientific, LLC., Denver, Colorado, USA

2) Quintessa, Ltd., Nottingham, UK

3) Japan Nuclear Cycle Development Institute Tokai Works, Tokai-Mura, Ibaraki, Japan

Table of Contents

Page

1 Introduction 1
2 Objectives 3
3 Data Compilation Procedure 4
3.1 Experimental Techniques 4
3.1.1 Batch Reactors 4
3.1.2 Flow-Through Reactors 5
3.2 Complications in Interpreting Experimental Rate Data 5
3.3 Data-Selection Rationale 6
3.3.1 Status of Kinetic Data for Mineral-Water Reactions 7
4 Kinetic Data for Mineral-Water Reactions 8
4.1 Summary of Kinetic Equations 8
4.2 Kinetic Data 9
5 A Technique for Assessing the Validity of the Local Equilibrium Assumption in Geochemical Models of Groundwater Evolution 20
5.1 Description of the Technique 20
5.1.1 Background 20
5.1.2 Modeling Approach 23
5.1.2.1 Benchmark of the approach 24
5.1.2.2 Practical constraints in using the modeling approach to estimate t_{eq} and l_{eq} 27
5.1.2.2.1 Conditional dependence of t_{eq} and l_{eq} on uncertainties in the saturation index 27
5.1.2.2.2 Longevity of stationary-state conditions 29
5.1.2.2.3 l_{eq} vs characteristic length scales in groundwater evolution models 30
5.1.2.2.4 Disparity between laboratory and field measurements of dissolution rates 30
5.2 Validity of the LEA in Geochemical Models of Groundwater Evolution at the Kamaishi Site 31
5.2.1 Conceptual Model 31
5.2.1.1 Fracture mineralogy 31
5.2.1.2 Surface area 32
5.2.1.3 Initial groundwater chemistry 33
5.2.1.4 Kinetic and thermodynamic data 33
5.2.1.5 Excluded phases 33
5.2.2 Reaction-Path Simulations 34
5.2.2.1 Nominal dissolution behavior 34
5.2.2.2 Field *vs.* laboratory dissolution rates 38
5.2.3 Summary 38
5.3 Estimated Migration Velocities of Oxidizing Fronts 40
5.3.1 Analytical Model of Redox-Front Migration 41
5.3.1.1 Previous applications of the model 42
5.3.2 Conceptual Model 43
5.3.2.1 Redox reactions 44
5.3.2.2 Initial concentrations of reactants 44
5.3.3 Estimated Redox-Front Velocities 45

5.3.3.1 Front retardation factors....45
5.3.3.2 Travel time estimates for oxidizing fronts to migrate 1000 m....45
5.3.4 Summary....46
6 Summary and Conclusions....47
7 References....49
Appendix: Analytical Model of Redox-Front Velocities....59

1 Introduction

The Japanese repository concept for permanent disposal of high-level nuclear wastes is based on an integrated system of natural and engineered barriers to radionuclide migration. A crystalline or sedimentary host rock (into which the wastes will be emplaced at depths of 1000 m, or 500 m, respectively) will function as the natural barrier. Engineered barriers will include a bentonite buffer, steel canister and vitrified-glass waste form. The natural and engineered barriers will act in concert, such that the wastes are isolated from the geosphere for long periods of time (*e.g.*, 1000 years), and subsequent releases of radionuclides to the biosphere are below levels that would pose an unacceptable risk to the public's health.

The Japan Nuclear Cycle Development Institute (JNC) is carrying out an applied R&D program to evaluate the feasibility of this concept[1]. The program utilizes the results of JNC's field studies of various geologic systems (Tono, Kamaishi and Mobara sites) and results of laboratory investigations of chemical and transport phenomena (ENTRY and QUALITY facilities) to build confidence in the results of modeling-based assessments of repository performance (PNC, 1992).

Geochemical models are an integral part of this work because they are used to interpret the results of field and laboratory studies, and to predict the future evolution of conditions in the near field and geosphere. JNC has for this reason devoted considerable effort over the past several years in developing reliable thermodynamic databases to support such models. Results include the development of two thermodynamic databases appropriate for geologic systems (Arthur *et al.*, 1999) and a compilation of thermodynamic data for hyperalkaline (*e.g.*, cementitious) environments (Savage *et al.*, 1999).

Kinetic data for mineral-water reactions are compiled in the present report. The data, including rate constants, reaction orders and activation energies, are compatible with a rate law consistent with surface reaction control and transition-state theory that is incorporated in two popular geochemical software packages: EQ3/6 (Wolery, 1992) and the Geochemist's Workbench (GWB; Bethke, 1996). The data are self-consistent in the sense that all values refer to far-from-equilibrium conditions where interpretations of experimental results are uncomplicated by the effects of variations in solution composition on reaction rates, methods used to estimate activity coefficients, and choices of thermodynamic data and standard states.

It may be necessary to incorporate kinetic data in geochemical models because natural systems are often in a state of partial equilibrium (Thompson, 1959). Partial equilibrium refers to a system that is in equilibrium with respect to at least one reversible reaction, but not with respect to others. A state of partial equilibrium in geologic systems is generally determined by the slow dissolution/precipitation rates of minerals because most aqueous reactions (excluding some oxidation-reduction reactions) are fast by comparison.

---

[1] JNC was established in 1998, and is responsible for many of the repository R&D functions formerly assigned to the Power Reactor and Nuclear Fuel Development Corporation (PNC).

Although it may be necessary to account for kinetic reactions in geochemical models, it is convenient to assume whenever possible that such reactions are under local-equilibrium control. Local equilibrium refers to the state of a system where phases in contact with one another react reversibly in response to changes in chemical potential, temperature or pressure. The thermodynamic, mathematical and numerical evaluation of geochemical models is greatly simplified when local equilibrium is assumed. This assumption is required if kinetic data for reactions considered in the model are unavailable.

To assess whether local equilibrium can be assumed in geochemical models of groundwater evolution, we describe an approach accounting for coupled fluid flow and water-rock interaction that can be used to estimate spatial and temporal scales of local equilibrium. The approach is demonstrated for conditions at JNC's Kamaishi *in-situ* tests site, and is also used to estimate the travel time necessary for oxidizing surface waters to migrate to repository levels. The estimated travel times support analyses of the *natural events scenario*, which JNC may consider in assessments of repository performance.

The objectives of the report are summarized below (Section 2), and this is followed in Section 3 by a brief description of the approach used to compile kinetic data retrieved from experimental studies described in the scientific literature. Tables of the kinetic parameters noted above are included in Section 4 for hydrolysis reactions involving feldspars, sheet silicates, zeolites, oxides, pyroxenes and amphiboles, and dissolution/precipitation reactions involving calcite and pyrite. The approach for assessing whether local equilibrium can be assumed in geochemical models of groundwater evolution, and for estimating travel times for oxidizing surface waters to migrate to repository depths, is discussed in Section 5. Conclusions are summarized in Section 6.

2 Objectives

The objectives of this investigation are:

- to compile kinetic data for mineral-fluid reactions,
- to describe and demonstrate a technique to estimate time and length scales necessary for the local equilibrium assumption (LEA) to be valid, and
- to estimate redox-front velocities and associated travel times for oxidizing conditions to be propagated to repository depths.

The first objective is necessary because a single source of self-consistent kinetic data that are compatible with the transition-state rate law in EQ3/6 and GWB is presently unavailable. The second objective is important because the technique can be used to determine whether kinetic data are needed for one or more reactions in geochemical models of groundwater chemistry and evolution. The technique, based on the stationary-state approximation to coupled fluid flow and water-rock interaction, is used to estimate spatial and temporal scales corresponding to local equilibrium conditions. Stationary-state behavior requires that reaction fronts are propagated at a constant velocity relative to the Darcy flow velocity, and that the front velocity is independent of reaction kinetics. These observations provide a basis for estimating the travel time necessary for a redox front, generated by the interaction of oxidizing surface waters with reducing minerals in a fracture, to migrate 1000 m. This distance represents the shortest possible distance between the surface and a HLW repository in crystalline rock.

3 Data Compilation Procedure

All the kinetic parameters in Section 4 are retrieved from experimental investigations of mineral dissolution behavior. Interpretations of experimental results are often equivocal, however, for reasons that can be traced to difficulties in adequately constraining experimental variables. Experimental techniques that have been used to generate kinetic data are briefly reviewed in Section 3.1, and potential sources of confusion in retrieving kinetic parameters from experimental results are summarized in Section 3.2. The rationale for selecting the data described in Section 4 is noted in Section 3.3, where remarks concerning the overall status of kinetic studies are also summarized.

3.1 Experimental Techniques

Rates of mineral dissolution are determined using *batch* or *flow-through* reactors. Experiments involving batch reactors are described, for example, by Grandstaff (1977), Rimstidt and Barnes (1980) and Schott *et al.* (1981). Posey-Dowty *et al.* (1986) provide an overview of experimental approaches using flow-through reactors, of which continuously-stirred tank reactors (CSTR; Rimstidt and Dove, 1986), fluidized-bed reactors (Chou and Wollast, 1985), and plug-flow reactors (Hill, 1977) are the most commonly used types.

3.1.1 Batch Reactors

Batch reactors are closed-system vessels containing a sample of the mineral and an aqueous solution. The solution, which is continuously agitated or stirred, may be equilibrated with the ambient atmosphere or other gases during the experiment. The dissolution rate is calculated by monitoring changes as a function of time in the concentrations of dissolution products. Solution compositions may be corrected for the effects of periodic sample removal during monitoring. Buffers may be used to minimize fluctuations in pH and ionic strength, and the solution may be changed periodically to prevent the composition from drifting over too large a range. The dissolution rate can be expressed as either the release rate of a given component, such as silica, or as the dissolution rate of the mineral itself. The rates are usually normalized per unit surface area, or mass, of the mineral.

The main disadvantage of using batch reactors in kinetic studies is the possibility that the dissolution rate may change with time due to variations in solution chemistry, or because minerals other than the investigated phase precipitate. Variations in solution parameters such as pH and Al concentration complicate interpretations of the experimental data because several variables change simultaneously. Precipitation of secondary phases is a particularly severe problem at moderate pH, where the solution commonly supersaturates with respect to minerals such as gibbsite and kaolinite, in which case experimental results provide only a minimum estimate of the dissolution rate.

3.1.2 Flow-Through Reactors

Flow-through reactors are used to investigate dissolution behavior under conditions of fixed solution chemistry. Continuous flow of fluid through the reactor ensures that the experiments remain undersaturated with respect to secondary phases, and allows for systematic manipulation of input solute concentrations. The composition of solutions sampled at the outlet is identical to solutions in contact with the mineral because the reactor is well mixed.

In CSTR-type reactors a sample of the mineral is placed in the reactor's tank and fluid is continuously pumped through the tank at flow rate Q. The reactor is stirred by a propeller or by agitation. The reaction rate, R, given by:

$$R = \frac{Q(C_o - C_i)}{A_s m}, \tag{3.1.2.1}$$

where A_s denotes the specific surface area (*i.e.*, per unit mass) and m refers to the mineral's initial mass, is determined by comparing the inlet concentration, C_i, with the outlet concentration, C_o, of a component dissolved from the mineral. Experiments using CSTR reactors are carried out until the outlet concentration reaches a constant value. The corresponding dissolution rate is referred to as the steady-state rate, which denotes the observed rate with respect to the composition of the solution as measured at the outlet. Any significant variations in the mass of the mineral during the experiment must be accounted for when determining the rate.

Fluidized-bed reactors are similar to CSTR reactors, but two flows rather than one are passed through the tank. One flow provides a single-pass of solution through the system. The other is a recirculating flow that stirs the mineral powder. The recirculating flow is sufficiently fast to continuously suspend particles in the reactor. Inlet and outlet concentrations are determined in samples from the single-pass flow, and results are analyzed using Eqn. (3.1.2.1).

Plug-flow reactors are more closely analogous to natural systems than CSTR and fluidized-bed reactors, but results are often more difficult to interpret. Operation of these reactors involves passing a solution through a packed bed of mineral grains. Ideally, each packet of fluid spends the same amount of time inside the reactor, given by ratio of the pore volume to the fluid-flow rate. The reaction rate is proportional to the difference in outlet and inlet concentrations of a component released from the mineral by dissolution, assuming volume changes due to reaction, radial flow and pooling of fluid in dead-end pore spaces are negligible. Interpreting rate data from the results of plug-flow experiments is especially difficult, however, because solution compositions vary as a function of location, and because secondary minerals may precipitate at various locations in the packed bed.

3.2 Complications in Interpreting Experimental Rate Data

Complications in retrieving rate data from experimental results stem from the number of factors that must be considered. The most intensively studied factors are the effects of temperature and pH on the dissolution rate. Other factors might include the catalytic or inhibiting effect of inorganic and organic solutes, the effect of saturation state of the solution, the types and concentrations of structural defects, and compositional variations within the mineral.

Uncertainties and ambiguities in interpreting the results of kinetic experiments arise from difficulties in adequately characterizing factors that affect the dissolution rate (*e.g.*, Posey-Dowty *et al.* (1986); Brantley and Chen, 1994). Dissolution may be interface- or transport-controlled, for example, and the rate-controlling mechanism may therefore depend on the stirring or agitation rate. The mechanism for a given reaction may be transport-controlled in a plug-flow reactor where fluid-flow rates are generally low, but interface-controlled in fluidized-bed reactors where the relatively rapid flow of recirculating fluids should minimize formation of thick hydrodynamic boundary layers. On the other hand, abrasion of particles in fluidized-bed reactors may cause the specific surface area to change during the experiment. This should not occur in CSTR experiments, but the comparatively low flow rate used in these experiments may cause fluids to stagnate near grain surfaces.

Another source of uncertainty in interpreting the results of kinetic studies is related to experimental difficulties in attaining steady-state concentrations. This may be caused by an extremely low dissolution rate, or to changes during the experiment in surface area or other surface properties, such as defect concentrations or concentrations of sorbed species. Uncertainties may also be generated by non-stoichiometric dissolution, caused either by precipitation of secondary phases or accelerated leaching of certain elements out of the mineral's structure. Non-stoichiometric behavior may be inferred from the chemistry of outlet solutions, but co-dissolution of impurity phases could also affect the composition of these solutions. Impurity phases may be intimately inter-mixed with the mineral of interest, and therefore difficult to detect or remove by hand picking. The presence of ions in solution that catalyze or inhibit the reaction rate may be produced by dissolution (*e.g.*, Al) or introduced by the experimenter in an effort to buffer solution compositions. These effects can only be detected if complete chemical analyses of the outlet solution are available.

Probably for the reasons noted above and others, discrepancies are not uncommon among kinetic data retrieved for the same reaction from several different experimental investigations. Different studies may treat starting materials differently (*e.g.*, in methods used to prepare mineral surfaces), determine mineral surface areas differently, use mineral names that are inconsistent with the actual composition, or account for precipitation of secondary phases with varying levels of rigor. Moreover, many experimental studies do not produce useful rate data. Studies that fail to determine surface areas or pH, to account for precipitation of secondary phases, to document variations in solution composition as a function of time, or to allow the reactions to occur for a sufficient period of time, are inadequate for the retrieval of meaningful rate data.

3.3 Data-Selection Rationale

Due to the complications noted above in interpreting the results of experimental kinetic studies, and due to the limited scope of the present investigation, it is not possible to carry out a critical evaluation of the available rate data for dissolution reactions. Also for these reasons, the alternative approach of simply compiling all reported values is unsatisfactory, because discrepancies among the data are not uncommon, as noted above, and in such cases it is not possible to decide which value, if any, is actually correct.

We instead accept the results of a limited number of recently published critical evaluations of kinetic data that focus on specific mineral groups. These studies include kinetic data for feldspars (Blum and Stillings, 1994), sheet silicates and related compounds (Nagy, 1994), and pyroxenes and amphiboles (Brantley and Chen, 1994). Kinetic data reported by these authors are included in tables in Section 4. Supplementary data from a limited number of other sources are also included in these tables if there is evidence that the data are retrieved with due regard of the complications noted in Section 3.2.

The studies by Blum and Stillings (1994), Nagy (1994), and Brantley and Chen (1994) retrieve kinetic data from published experimental results using empirical rate laws, such as:

$$R = k a_{H^+}^n , \tag{3.3.1}$$

where R denotes the dissolution rate normalized per unit surface area (mol m^{-2} sec^{-1}), k refers to the rate constant (mol m^{-2} sec^{-1}), a_{H+} represents the activity of the hydrogen ion and n stands for an adjustable parameter. Both k and n are determined in these studies by regression of one or more sets of experimental data. Blum and Stillings (1994) determine k and n as a function of temperature and evaluate results to determine consistent values of the activation energy. Ranges of activation parameters reported in the literature are documented by Brantley and Chen (1994) and Nagy (1994).

We note that if both sides of Eqn. (3.3.1) are multiplied by the surface area, s (m^2), the resulting equation is *mathematically* equivalent to the transition-state rate law in EQ3/6 and GWB, *under far-from-equilibrium conditions* [see Eqn. (4.1.4), Section 4.1]. Strictly for modeling purposes therefore, values of k and n reported by Blum and Stillings (1994), Nagy (1994) and Brantley and Chen (1994) are interchangeable with rate-constant and reaction-order terms, respectively, that appear in kinetic equations solved by EQ3/6 and GWB. These parameters may in fact also be conceptually consistent with the transition-state rate law over the full range of conditions from irreversible to reversible reaction, but it is important to note that the empirical rate laws, as such, are unconstrained by any specific reaction mechanism.

3.3.1 Status of Kinetic Data for Mineral-Water Reactions

Kinetic data for mineral-water reactions are still limited. Critically evaluated data for dissolution reactions involving 34 minerals are compiled in Section 4. Similar data for precipitation reactions are unavailable, with the single exception of calcite. Much of the dissolution data is strictly valid only for reactions in acidic solutions, and these data are therefore probably irrelevant for most calculations pertaining to HLW disposal.

4 Kinetic Data for Mineral-Water Reactions

Kinetic data compatible with the transition-state rate law adopted in EQ3/6 and GWB to describe dissolution/precipitation rates of minerals in geologic systems are compiled in this section. Kinetic equations describing this rate law are summarized in Section 4.1, and associated data are tabulated in Section 4.2. The tabulations include reaction rate constants, reaction orders and activation energies that are based on experimental measurements as reported in the literature. The data are self-consistent in the sense that all values refer strictly to far-from-equilibrium conditions, where interpretations of experimental results are uncomplicated by the effects on reaction rate of variations in solution composition, choices of thermodynamic data and standard states, and methods used to estimate activity coefficients.

4.1 Summary of Kinetic Equations

The kinetic data described below are compatible with a general rate law for hydrolysis reactions that is consistent with surface reaction control and transition state theory. It is represented by (*e.g.*, Murphy and Helgeson, 1989):

$$-\frac{dn}{dt} = ksa_{H^+}^{n_{H^+}}\left[1-\exp(-A/\sigma RT)\right], \tag{4.1.1}$$

where n denotes the number of moles of reactant mineral in the system, k stands for the rate constant[2] (which may include such parameters as adsorption and hydrolysis equilibrium constants, activity coefficients for surface species, *etc.*), s refers to the total surface area corresponding to a reference volume (*e.g.*, 1000 cm^3) of aqueous solution, n denotes the reaction order with respect to the activity (a) of the hydrogen ion, A represents the chemical affinity for the overall reaction, σ stands for the ratio of the rate of decomposition of the activated complex to that of the overall reaction (usually taken as being equal to one), R refers to the gas constant and T denotes temperature. The chemical affinity for the overall reaction is given by:

$$A = RT\ln(K/Q), \tag{4.1.2}$$

where K stands for the equilibrium constant and Q refers to the activity product. Assuming $\sigma = 1$, Eqn. (4.1.1) can be rewritten as:

$$-\frac{dn}{dt} = ksa_{H^+}^{n_{H^+}}\left(1-\frac{Q}{K}\right), \tag{4.1.3}$$

[2] Murphy and Helgeson (1989) refer to this parameter as the operational rate constant because it can be calculated directly from experimental data.

Note that if the ratio Q/K > 1, the aqueous solution is supersaturated and Eqn. (4.1.3) then defines the precipitation rate. For dissolution reactions under far-from-equilibrium conditions, *i.e.*, when $Q << K$, the reaction rate is given to a good approximation by:

$$-\frac{dn}{dt} = ksa_{H^+}^{n_{H^+}}. \tag{4.1.4}$$

The rate constants tabulated in Section 4.2 are strictly compatible only with Eqn. (4.1.4), because they are generally calculated from experimental data referring to far-from-equilibrium conditions, where the effects on reaction rate of the affinity term in Eqn. (4.1.1) are negligible. These constants may be used with caution in calculations considering near-to-equilibrium conditions, but original data sources should be consulted to determine whether the rate under such conditions is affected by the presence of aqueous species that may inhibit or catalyze the reaction.

Temperature effects on the rate constant are calculated using a modified Arrhenius relation (*e.g.*, Murphy and Helgeson, 1989):

$$\frac{d\ln(k/T)}{d(1/T)} = \frac{-\Delta H'}{R}, \tag{4.1.5}$$

where $\Delta H'$ stands for the activation enthalpy. Integration of Eqn. (4.1.5) at constant pressure (or assuming that k is pressure independent) and assuming $\Delta H'$ is temperature independent gives the result:

$$k = \frac{Tk^0}{T^0}\exp\left[\left(\frac{-\Delta H'}{R}\right)\left(\frac{1}{T} - \frac{1}{T^0}\right)\right], \tag{4.1.6}$$

where $k^0 = k$ at T^0.

Activation energies, E_A, rather than activation enthalpies are provided in the tables in Section 4.2. Activation enthalpies are readily calculated using the relation:

$$\Delta H' = E_A - RT. \tag{4.1.7}$$

Rate constants calculated using Eqns. (4.1.6) and (4.1.7) at temperatures exceeding the experimentally calibrated range of activation energies should be used with caution.

4.2 Kinetic Data

4.2.1 Silicate Minerals and Related Compounds

Kinetic data for hydrolysis reactions involving feldspars, sheet silicates, zeolites, oxides, pyroxenes and amphiboles are summarized in Tables 4.2.1_1 – 4.2.1_6. Most of the data are from Blum and Stillings (1994), Nagy (1994) and Brantley and Chen (1994). Each of these references includes a thorough review of the available experimental data for the

minerals considered, and describes potential sources of uncertainty and ambiguity in the authors' interpretations of experimental results.

Rate constants and reaction orders for feldspar dissolution are given in Table 4.2.1_1, which is based primarily on the critical evaluation of experimental data carried out by Blum and Stillings (1994). The data refer to acidic, neutral or basic solutions, where respective statements of Eqn. (3.3.1) (see Section 3) adopted by these authors are:

$$R = ka_{H^+}^{-n},$$

$$R = k, \text{and}$$

$$R = ka_{OH^-}^{n},$$

Rate constants and reaction orders listed in Table 4.2.1_1 are mathematically consistent with the rate law represented by Eqn. (4.1.4). They may also be conceptually consistent with the general rate law [Eqn. (4.1.1)] incorporated in EQ3/6 and GWB. Activation energies reported in the literature or estimated by Blum and Stillings (*op. cit.*) are documented in Table 4.2.1_2.

Rate constants and reaction orders for dissolution of sheet silicates, zeolites and related compounds (brucite, gibbsite, quartz and moganite) at 25°C are summarized in Table 4.2.1_3. Most of these data are based on the critical evaluation of experimental data carried out by Nagy (1994), who adopted the empirical rate law represented by Eqn. (3.3.1). Rate constants and reaction orders listed in Table 4.2.1_3 are mathematically consistent with the rate law represented by Eqn. (4.1.4). They may also be conceptually consistent with the general rate law given by Eqn. (4.1.1). Activation energies are summarized in Table 4.2.1_4.

Rate constants and reaction orders for dissolution of pyroxenes and amphiboles at 25°C are summarized in Table 4.2.1_5. These data are taken from the critical evaluation of experimental data carried out by Brantley and Chen (1994), who adopted the empirical rate law represented by Eqn. (3.1.3). Rate constants and reaction orders listed in Table 4.2.1_5 are mathematically consistent with the rate law represented by Eqn. (4.1.4). They may also be conceptually consistent with the general rate law given by Eqn. (4.1.1). Activation energies reported in the literature are tabulated in Table 4.2.1_6.

Table 4.2.1_1: Rate constants and reaction orders for feldspar dissolution.

Feldspar[a]	*log k* (*mol m^{-2} sec^{-1}*)	*n*	*T(°C)*	*pH*	*Reference*
Acidic Solutions: Rate (mol m^{-2} sec^{-1}) = $k\,(a_H^+)^{-n}$					
Albite	-10.04	0.5	6.6	3	Chou (1985)
	-9.66	0.5	25	3	〃
	-9.64	0.5	26.2	3	〃
	-9.4	0.5	35	3	〃
	-9.37	0.5	39	3	〃
	-9.19	0.5	45	3	〃
	-9.11	0.5	50	3	〃
	-9.00	0.5	55	3	〃
	-8.7	1	25	1 - 3	Murphy and Helgeson (1989)[2]
	-9.69	0.49	25	≤ 5	Wollast and Chou (1985)
	-8.18	0.97	70	≤ 3	Knauss and Wolery (1986)
	-9.5	0.5	25	acid	Sverdrup (1990)
	-10.2	0.5	8	acid	〃
	-8.5	0.2	100	≤ 5	Hellmann (1994)
	-5.9	0.4	200	≤ 5	〃
	-4.1	0.6	300	≤ 5	〃
K-feldspar	-9.45	0.4	25	acid	Holdren and Spyer (1985;1987)
	-9.07	0.68	70	1 - 3.6	Bevan and Savage (1989)
	-8.28	0.85	95	1 - 3.6	〃
	-10.45	0.5	5	acid	Schweda (1990)
	-10.15	0.5	15	acid	〃
	-9.93	0.5	25	1 - 5.7	〃
	-9.55	0.5	35	acid	〃
	-9.12	0.5	50	acid	〃
	-8.55	0.5	70	acid	〃
	-8.7	1	25	1 - 3	Murphy and Helgeson (1987)[2]
	-9.6	0.5	25	acid	Sverdrup (1990)
	-10.3	0.5	8	acid	〃
Labradorite	-8.86	0.5	25	1 - 5	Sjöberg (1989)
	-7.37	0.5	70	1 - 2	〃
	-9.20	0.5	15	1 - 2	〃
	-8.93	0.5	25	acid	Sverdrup (1990)
	-9.67	0.5	8	acid	〃
	-8.29	0.41	25	3.1 - 5.3	Welch and Ullman[5]
	-9.33	0.4	25	2 - 5.1	Oxburgh *et al.* (1994)
Anorthite	-4.47	1.12	25	2	Fleer (1982)
	-3.82	1.12	50	2	〃
	-3.62	1.14	70	2	〃
	-5.87	1.12	25	≤5	Brady and Walther (1989); Holdren and Spyer (1985); Amrhein and Suarez (1988)
	-5.48	0.95	25	2.2 - 5	Sverdrup (1990)
	-3.13	1.5	45	2.4 - 3.1	Oelkers and Schott (1995)
	-2.98	1.5	60	2.4 - 3.1	〃
	-2.84	1.5	75	2.4 - 3.1	〃
	-2.72	1.5	95	2.4 - 3.1	〃
Neutral Solutions; Rate (mol m^{-2} sec^{-1}) = k					
Albite	-8.8	0.26	90	3 - 5	Voigt *et al.* (unpub.)
	-12.15	0	25	5 - 8	Wollast and Chou (1985)
	-11.14	0	70	4 - 8.8	Knauss and Wolery (1986)

Feldspar[a]	*log k* (*mol m*$^{-2}$ *sec*$^{-1}$)	*n*	*T*(°C)	*pH*	*Reference*
	-11.8	0	25	neutral	Sverdrup (1990)
	-12.4	0	8	neutral	〃
	-11.5	0	25	3 - 8	Murphy and Helgeson (1989)[2]
	-9.5	0	100	5 - 8.6	Hellmann (1994)
	-7.7	0	200	5 - 8.6	〃
	-6.2	0	300	5 - 8.6	〃
K-feldspar	-11.5	0	25	3 - 8	Murphy and Helgeson (1989)[2]
Basic Solutions; Rate (mol m^{-2} sec^{-1}) = $k(a_{OH^-})^n$					
	-9.95	0.3	25	>8	Wollast and Chou (1985)
	-9.25	0.48	70	>8.8	Knauss and Wolery (1986)
	-9.9	0.3	25	basic	Sverdrup (1990)
	-10.3	0.3	8	basic	〃
	-8.3	0.3	100	≥8.6	Hellmann (1994)
Albite	-6.3	0.4	200	≥8.6	〃
	-4.5	0.6	300	≥8.6	〃
	-8.3[3]	0.3	150	9	Oelkers *et al.* (1994)
	-8.71[3]	0.3	150	9	〃
	-9.16[3]	0.3	150	9	〃
	-10.43[4]	0.45	25	basic	Schweda (1990)
	-10.2[4]	0.45	25	basic	〃
	-9.8[4]	0.73	25	basic	〃
	-9.2	0.3	25	basic	Sverdrup (1990)
K-feldspar	-9.6	0.3	8	basic	〃
	-6.15[3]	0.3	150	9	Gautier *et al.* (1994)
	-6.48[3]	0.3	150	9	〃
	-7.33[3]	0.3	150	9	〃

1- nominal structural formulas: albite (Ab), $NaAlSi_3O_8$; anorthite(An), $CaAl_2Si_2O_8$; oligoclase, Ab90An10 – Ab70An30; labradorite, Ab50An50 – Ab30An70; K-feldspar, $KAlSi_3O_8$.
2- retrieved using data reported by Helgeson *et al.* (1984);
3- log *k* estimates vary with chemical affinity.
4- log *k* and *n* depend on Li concentration.
5- reported by Blum and Stillings (1994)

Table 4.2.1_2: Activation energies for feldspar dissolution reactions.

Feldspar	E_a *(kJ mol^{-1})*	*pH*	*Temp. range (°C)*	*Reference*
Albite	84	acid	25 - 200	Helgeson *et al.* (1984)
	58.6	pH 3	6.6 - 55	Chou (1985)
	117	< 3	25 - 70	Knauss and Wolery (1986)
	54.4	neutral	〃	〃
	32.2	basic	〃	〃
	64.3	acid	not reported	Sverdrup (1990)
	50.7	neutral	〃	〃
	59.3	basic	〃	〃
	71.4	pH 1.4	25 - 90	Rose (1991)
	62.8	acid	5 – 300	Chen (1994)
	88.9	acid	100 - 300	Hellmann (1994)
	68.8	neutral	〃	〃
	85.2	basic	〃	〃
	88.7	acid	---	Murphy and Helgeson (1989)[1]
	37.8	neutral	---	〃
	44.0[2]	pH 3	5 - 90	Stillings *et al.* (1995b)
	60.0	acid	5 - 300	Blum and Stillings (1994)
	67.7	neutral	〃	〃
	50.1	basic	〃	〃
K-feldspar	38	neutral	25 - 200	Helgeson *et al.* (1984)
	14.4 – 57.7	1 – 3.6	70 - 90	Bevan and Savage (1989)
	52 - 60	3 - 4	5 - 70	Schweda (1990)
	63 - 70	10.9	〃	〃
	53 – 78.3	acid	not reported	Sverdrup (1990)
	35 - 37	neutral	〃	〃
	81.9	acid	---	Murphy and Helgeson (1989)[1]
	51.7	acid	5 - 100	Blum and Stillings (1994)
	57.8	basic	〃	〃
Oligoclase	80.3	acid	not reported	Sverdrup (1990)
	46.1	neutral	〃	〃
Labradorite	65	1 - 2	15 - 70	Sjöberg (1989)
	48.1[3]	4	21 - 60	Brady and Carroll (1994)
	66.4	acid	5 - 70	Blum and Stillings (1994)
Anorthite	33	2	25 - 70	Fleer (1982)
	35	acid	not reported	Sverdrup (1990)
	107	neutral	〃	〃
	80.7	acid	25 - 95	Blum and Stillings (1994)

1- retrieved using data reported by Helgeson *et al.* (1984);
2- experiments conducted in 10^{-3} M oxalic acid;
3- experiments conducted in 10^{-3} M acetic acid

Table 4.2.1_3: Rate constants and reaction orders for dissolution of sheet silicates, zeolites and related compounds at 25°C[1].

Mineral[2]	*log k* ($mol\ m^{-2}\ sec^{-1}$)	*n*	*pH range*	*Reference*
Brucite	-7.72	-0.5	1 - 5	Vermilyea (1969)
Gibbsite	-11	0.3	3.3 - 5	Mogollon *et al.* (1994)
Quartz	-13.8	0	---	Murphy and Helgeson (1989)[3]
〃	-14.1	0	3.5	Gislason *et al.* (1997)
〃	-12.3	0	neutral	Dove and Crerar (1990)
Moganite	-12.8	0	3.5	Gislason *et al.* (1997)
Amorph. SiO_2	-10.7	0.74	0 - 3	Plettinck *et al.* (1994)
〃	-14.5	-0.52	3 - 6	〃
Kaolinite	-12.6	0.09	0.5 - 6	Carroll and Walther (1990)
〃	-12.9	-0.09	4 – 6.5	Wieland and Stumm (1992)
〃	-15.3	-0.25	7.5 - 12	Carroll and Walther (1990)
Chrysotile	-12.0	0[4]	2.1 – 5.7	Bales and Morgan (1985)
〃	-13.8	-0.19	8.5 - 11	〃
Talc	-12.0	0	5	Lin and Clemency (1981c)
Montmorillonite[5]	-11.5	0.38	1 - 5	Furrer *et al.* (1993)
〃	-16.3	-0.13	6 - 10	Heydemann (1966)
Muscovite	-12.5	0.1	3 - 5	Stumm *et al.* (1987)[8]
〃	-13.2	-0.1	5.6 – 10.6	Nickel (1973)
〃	-11.8	0.14	1 - 4	Kalinowski and Schweda (1996)
Illite	-14.9	0.02	acidic	Nagy (1994)[6]
〃	-14.9	-0.11	basic	〃
Biotite	-10.5	0.34	3 - 7	Acker and Bricker (1992)
〃	-9.5	0.61	1 - 4	Kalinowski and Schweda (1996)
Phlogopite	-7.12	1	3.3 – 5.3	Lin and Clemency (1981a)
〃	-10.5	0.4	1 - 4	Kalinowski and Schweda (1996)
Chlorite	-15	-0.5	3.1 – 5.2	May *et al.* (1995)
Laumontite	-12.3	0	basic	Savage *et al.* (1993)
Heulandite	-7.7	0.7	2 – 5.8	Ragnarsdottir (1993)
〃	-11.8	0	5.8 – 7.2	〃
〃	-14.3	-0.3	7.2 – 12.2	〃
Analcime	-11	---[7]	9	Murphy *et al.* (1996)
Na-Clinoptilolite	-13.15	---[7]	9	〃

1- based on release rates of silica, except for brucite (Mg) and gibbsite (Al); dissolution of 2:1 layer silicates normalized to the $O_{10}(OH)_2$ formula unit.

2- nominal structural formulas: brucite, $Mg(OH)_2$; gibbsite, $Al(OH)_3$; quartz, moganite, amorphous SiO_2, SiO_2; kaolinite, $Al_2Si_2O_5(OH)_4$; chrysotile, $Mg_3Si_2O_5(OH)_4$; talc, $Mg_3Si_4O_{10}(OH)_4$; montmorillonite, Swy-1; illite, Fithian; biotite, $K(Mg,Fe^{2+})_3(Al,Fe^{3+})Si_3O_{10}(OH,F)_2$; phlogopite, $KMg_3Si_3AlO_{10}(F,OH)_2$; laumontite, $CaAl_2Si_4O_{12}\cdot 4H_2O$; heulandite, $(Na,Ca)_{2-3}Al_3(Al,Si)_2Si_{13}O_{36}\cdot 12H_2O$; analcime, $NaAlSi_2O_6.H_2O$; Na-clinoptilolite, $(Na,K,Ca)_{2-3}Al_3(Al,Si)_2Si_{13}O_{36}\cdot 12H_2O$.

3- calculated based on experimental data from Rimstidt and Barnes (1980).

4- reaction order from Hume and Rimstidt (1992);

5- SWy-1 montmorillonite, reaction order based on data from batch (closed-system) experiments;

6- recalculated by Nagy (1994) using experimental data from Heydemann (1966).

7- reaction order unspecified.

8- comparable with the reaction rate determined by Lin and Clemency (1981b) at pH 5.

Table 4.2.1_4: Activation energies for dissolution of sheet silicates and related minerals

Mineral	E_a ($kJ\ mol^{-1}$)	*pH*	*Temp (°C)*	*Reference*
Brucite	42	1 –3	25 - 75	Vermilyea (1969)
Gibbsite	68	1.75	25 - 55	Bloom (1983)
〃	60 - 67	1.75 – 2.19	10 - 40	Bloom and Erich (1987)
〃	60	2.27 – 2.93	〃	〃
〃	64	2.31	〃	〃
〃	56	3	25 - 80	Nagy and Lasaga (1992); Mogollon *et al.* (1994)
〃	92 - 97	13.8 - 15	35 - 65	Packter and Dhillon (1973)
〃	76 - 83	13.3 - 15	20 - 65	Packter and Dhillon (1974)
Quartz	67.4 – 76.6	---	0 - 300	Rimstidt and Barnes (1980)
〃	80.5 ± 1.9	3.5	25 - 200	Gislason *et al.* (1997)
〃	71.3 ± 8.7	neutral	25 - 300	Dove and Crerar (1990)
〃	77.8	---	0 - 300	Murphy and Helgeson (1989)[1]
Moganite	70.5 ± 4.5	3.5	25 - 200	Gislason *et al.* (1997)
Kaolinite	54	-0.7 - 1	0 - 50	Kline and Fogler (1981)
〃	67 → 7.1	1 - 7	25 – 80	Carroll and Walther (1990)
〃	29.3	3 - 4	25 - 80	Ganor *et al.* (1995)
〃	14.2 → 41	8 - 12	25 - 80	Carroll and Walther (1990)
Chrysotile	63 - 84	1	22 - 80	Thomassin *et al.* (1977)
Talc	42	-0.7 - 1	25 - 60	Kline and Fogler (1981)
Montmorillonite[1]	48	-0.7 - 1	0 - 25	〃
Muscovite	54	〃	38 - 70	〃
〃	22	3	25 - 70	Nickel (1973); Stumm *et al.* (1987); Knauss and Wolery (1989)
Illite	54	-0.7 - 1	0 - 45	Kline and Fogler (1981)
Phlogopite	29 - 42	2	50 - 120	Kuwahara and Aoki (1995)
Clinochlore	88	-0.3	20 - 60	Ross (1967)
Laumontite	58	basic	80 - 150	Savage *et al.* (1993)

[1] Swy-1

Table 4.2.1_5: Rate constants and reaction orders for dissolution of pyroxenes and amphiboles at 25°C.

Mineral	*log k* ($mol\ m^{-2}\ sec^{-1}$)	*n*	*pH*	*Reference*
Enstatite	-9.3 ± 0.7	-0.25± 0.14	2 - 7	Ferruzzi (1993)
Bronzite	-9.8±0.3	-0.49±0.13	< 5	Grandstaff (1977); Schott and Berner (1983)
Diopside	-9.6±0.2	-0.18±0.03	2 - 10	Knauss *et al.* (1993)
Diopside	-9.4±0.4	-0.22±0.1	2 - 6	Knauss *et al.* (1993)
Diopside	-10.2±0.2	-0.10±0.04	2 - 10	Knauss *et al.* (1993); Chen and Brantley[2]
Diopside	-10.2±0.2	-0.20±0.07	1 - 4	Chen and Brantley[2]
Diopside	-10.5±0.2	-0.20±0.06	1 - 4	Chen and Brantley[2]
Augite	-7.3±0.6	-0.99±0.14	< 6	Sverdrup (1990); Siegel and Pfannkuch (1984)
Wollastonite	-8.0±0.2	-0.24±0.04	≤ 7.2	Xie (1994)
Wollastonite	-11.6±0.6	0.27±0.07	≥ 7	Xie (1994)
Rhodonite	-9.3±0.3	-0.33±0.06	2.1 - 7.1	Banfield *et al.* (1995)
Spodumene	-4.6±0.4	-0.72±0.08	3 - 7	Sverdrup (1990)
Jadeite	-7.6±0.6	-0.30±0.12	3 - 6	Sverdrup (1990)
Anthophyllite	-12.3±0.1	-0.33±0.03	1 - 4	Chen and Brantley [2]
Anthophyllite	-12.2±0.007	-0.37±0.003	1 - 4	Chen and Brantley [2]
Tremolite	-11.5	0.11	1 - 6	Schott *et al.* (1981)
Hornblende	-8.9±0.2	-0.75±0.06	3.6 - 4	Zhang (1990)
Glaucophane	-6.4±0.3	-0.69±0.05	3 - 7	Sverdrup (1990)

1- nominal structural formulas: enstatite, $Mg_2Si_2O_6$; bronzite, $(Mg,Fe^{2+})_2Si_2O_6$; diopside. $CaMgSi_2O_6$; augite, $(Ca,Mg,Fe^{2+},Al)_2(Si,Al)_2O_6$; wollastonite, $CaSiO_3$; rhodonite, $(Mn,Ca,Fe)SiO_3$; spodumene, $LiAlSi_2O_6$; jadeite, $NaAlSi_2O_6$; anthophyllite, $(Mg,Fe^{2+})_7Si_8O_{22}(OH)_2$; tremolite, $Ca_2(Mg,Fe^{2+})_5Si_8O_{22}(OH)_2$; hornblende, $(Na,K)_{0-1}Ca_2(Mg,Fe^{2+},Fe^{3+},Al)_5Si_{6-7.5}Al_{2-0.5}O_{22}(OH)_2$; glaucophane, $Na_2Mg_3Al_2Si_8O_{22}(OH)_2$.

2- reported by Brantley and Chen (1994)

Table 4.2.1_6: Activation energies for dissolution of pyroxenes and amphiboles

Mineral	E_a *(kJ mol^{-1})*	*pH*	*Temp. range (°C)*	*Reference*
Enstatite	49	6	20 - 60	Schott *et al.* (1981)
Enstatite	41.2	4	25 - 65	Bailey (1974)
Bronzite	44.1	2.1	1 - 42	Grandstaff (1977)
Diopside	50 - 63	0 - 1	50 - 63	Sanemasa and Katsura (1973)
Diopside	50 - 150	1.7 - 4	20 - 60	Schott *et al.* (1981)
Diopside	38	4 - 6	not reported	Schott and Petit (1987)
Diopside	81	2	"	"
Diopside	40.6	2 - 12	25 - 70	Knauss *et al.* (1993)
Diopside	96.1	1 - 4	25 - 90	Chen and Brantley [1]
Augite	78	6	20 - 75	Schott and Berner (1985)
Augite	115.4	4	25 - 60	Brady and Carroll (1994)
Wollastonite	79.2	7	23.5 - 40	Rimstidt and Dove (1986)
Wollastonite	54.6	4	26 - 65	Bailey (1977)
Wollastonite	72	4	26 - 65	"
Anthophyllite	77.2	1 - 4	25 - 90	Chen and Brantley[1]
Forsterite	79.7	1.8 – 9.8	25 - 65	Wogelius and Walther (1992)

1- reported by Brantley and Chen (1994)

4.2.2 Calcite

Plummer *et al.* (1978) proposed an *activity-term* rate law for dissolution and precipitation of carbonate minerals given by:

$$-\frac{dn}{dt} = s\left(k_1 a_{H^+} + k_2 a_{H_2CO_3} + k_3 a_{H_2O} + k_4 a_{HCO_3^-}\right) \qquad (4.2.2.1)$$

where $k_{1...4}$ are empirical constants determined by regression of experimental data. Delany *et al.* (1986) demonstrated that experimental data on the precipitation kinetics of calcite (Reddy *et al.*, 1981) could be fit equally well using either Eqn. (4.2.2.1) or Eqn. (4.1.1). The rate constant in the latter equation providing the best fit of the experimental data was determined as:

$k = 7 \times 10^{-7}$ mol m^{-2} sec^{-1},

assuming $\sigma = 1$ and that the reaction order with respect to $H^+ = 0$. It is inferred that these data may be used in Eqn. (4.1.1) or (4.1.4) to calculate the dissolution and precipitation rate of calcite, but it is important to note that the rate constant was determined only by regression of experimental data on calcite precipitation.

4.2.3 Pyrite

A suitable form of the rate law represented by Eqn. (4.1.1) has not been determined for the aqueous oxidation of pyrite. Reaction fronts generated in part by this reaction in natural systems tend to be extremely sharp, however, suggesting that the product of the rate constant and surface area terms in Eqn. (4.1.4) are relatively large in comparison with the dissolution rate of silicate minerals. Lichtner and Waber (1992), for example, simulated the

formation of such sharp reaction fronts in a coupled fluid flow and water-rock interaction model of the migration of oxygenated surface waters through fractures at the Osamu Utsumi uranium mine, Pocos de Caldas, Brazil, by assuming the rate law given by Eqn. (4.1.4) with $k = 10^{-10}$ mol m^{-2} sec^{-1}, $s = 2$ m^2 l^{-1} and $n_{H+} = 0$. These data may thus constitute a reasonable first approximation of the aqueous oxidation rate of pyrite under far-from-equilibrium conditions.

4.2.4 Other Sources of Kinetic Data

A number of experimental studies have been carried out on the dissolution/precipitation rates of minerals not considered in Sections 4.2.1 – 4.2.3. These sources of data are not considered in the present study because retrieved values are inconsistent with the rate law described in Section 4.1.

The studies do, however, provide valuable information on the dissolution behavior of several minerals that could be important in geochemical models. A noteworthy example is the study by Williamson and Rimstidt (1994), who compiled rate data reported in the literature for the reaction of pyrite (FeS_2) at 25°C with dissolved oxygen,

$$FeS_2 + 7/2O_2(aq) + H_2O \rightarrow Fe^{2+} + 2SO_4^{2-} + 2H^+,$$

to produce a rate law that is applicable over four orders of magnitude in $O_2(aq)$ concentrations over the pH range 2-10. Their rate law is given by:

$$R = 10^{-8.19(\pm 0.10)} \frac{m_{O_2(aq)}^{0.51(\pm 0.04)}}{m_{H^+}^{0.11(\pm 0.01)}},$$

where R denotes the rate of pyrite destruction (mol m^{-2} sec^{-1}) and m refers to concentration (mol kg^{-1}).

Williamson and Rimstidt (*op. cit.*) followed a similar approach to develop rate laws for the reaction involving pyrite oxidation by Fe^{3+},

$$FeS_2 + 14Fe^{3+} + 8H_2O \rightarrow 15Fe^{2+} + 2SO_4^{2-} + 16H^+,$$

that are applicable over a six order of magnitude range of Fe^{3+} and Fe^{2+} concentration for the pH range ≈ 0.5 – 3. In anoxic (*i.e.*, N_2-purged) solutions, the rate of pyrite destruction (mol m^{-2} sec^{-1}) is given by:

$$R = 10^{-8.58(\pm 0.15)} \frac{m_{Fe^{3+}}^{0.30(\pm 0.02)}}{m_{Fe^{2+}}^{0.47(\pm 0.03)} m_{H^+}^{0.32(\pm 0.04)}},$$

and in solutions where dissolved oxygen is present, it is given by:

$$R = 10^{-6.07(\pm 0.57)} \frac{m_{Fe^{3+}}^{0.93(\pm 0.07)}}{m_{Fe^{2+}}^{0.40(\pm 0.06)}}.$$

In both cases, the rate is not influenced by SO_4^{2-}, Cl^- or ionic strength. It does depend on the presence (but not concentration) of $O_2(aq)$, however.

Other notable experimental kinetic studies are described by Rickard (1995) on the precipitation kinetics of FeS, Bruno *et al.* (1992) on the dissolution rate of hematite and White *et al.* (1994) on the dissolution kinetics of magnetite and ilmenite.

5 A Technique for Assessing the Validity of the Local Equilibrium Assumption in Geochemical Models of Groundwater Evolution

Geochemical models of groundwater evolution may require kinetic data such as described in Section 4 if the *local equilibrium assumption* (LEA) is invalid for the particular system being modeled. This assumption requires that disequilibrium conditions occurring along a groundwater flowpath instantaneously relax to an equilibrium state. In reality, this must occur over a finite flow-path distance and time, but the LEA is a good approximation if this distance and time are less than the scales of interest for the problem at hand (Knapp, 1989). The LEA is adopted whenever possible because it greatly simplifies thermodynamic, mathematical and numerical evaluation of geochemical models.

The LEA is adopted in JNC's geochemical models of generic groundwater types in Japan (Yui *et al.*,1999), and groundwater evolution models applied to the Tono (Sasamoto *et al.*, 1999a) Kamaishi (Sasamoto *et al.*, 1999b) and Mobara (Sasamoto *et al.*, 1999c) *in-situ* tests sites. To assess whether this assumption is reasonable for conditions considered in these models, we describe a technique based on the stationary-state approximation to coupled fluid flow and water-rock interaction that can be used to estimate distance and time scales necessary for the LEA to be valid. The technique is summarized in Section 5.1, and is demonstrated for conditions at the Kamaishi site in Section 5.2.

A consequence of stationary-state behavior is utilized in Section 5.3 to estimate the time required for oxidizing surface waters to migrate 1000 meters below the surface, which is the depth envisaged in Japan for a deep geologic repository for HLW in crystalline rock. Migration of oxidizing solutions to repository depths is one aspect of a *natural events* scenario that JNC may consider in assessments of repository performance.

5.1 Description of the Technique

5.1.1 Background

The stationary state approximation (Lichtner 1985; 1988) represents the evolution of chemical conditions in open multicomponent, multiphase systems in terms of a sequence of relatively long-lived stationary states of the system, which are linked in time by short-lived transients. Each stationary state is represented by spatially fixed reaction boundaries, and nearly constant mineral abundances, porosity, permeability, and reactive surface areas. A stationary state is an open-system analogue of an equilibrium state in closed systems insofar as both are independent of time. A stationary state, however, is not generally at equilibrium. Rather, its existence depends on the condition that mineral abundances, reactive surface areas, porosity and permeability vary slowly compared with the time required to form a stationary state. Such conditions are appropriate for geologic systems because the concentrations of aqueous species in a representative elemental volume of the system are much less than their concentrations in coexisting minerals.

The concept of a stationary state is illustrated schematically in Fig. 5.1.1_1, where it is assumed that a porous rock column consisting initially of K-feldspar and an equilibrated solution (a) begins to react with infiltrating rainwater that is not at equilibrium with K-feldspar. The first packet of rainwater displaces the equilibrated fluid and leaves behind reaction zones of gibbsite (starting at location $I^{(1)}_{\pi_1}$ and ending at $I^{(2)}_{\pi_1}$) and kaolinite (starting at location $I^{(1)}_{\pi_2}$ and extending downstream)(b). The gibbsite zone is stationary, but the kaolinite zone grows with time. The second and subsequent packets of rainwater interact with K-feldspar in exactly the same way as the first packet (c). The location of the gibbsite zone and beginning of the kaolinite zone consequently do not change with time, and appear to be stationary as long as associated changes in the porosity, volume fractions of reacting minerals, surface area and permeability are insignificant. Eventually, however, K-feldspar dissolves completely at the column inlet. The next fluid packet is undersaturated with respect to gibbsite when it reaches the previously deposited gibbsite zone, causing this mineral to dissolve at the upstream position of the zone and to precipitate further downstream (d). The initial stationary state of the system (Fig. 5.1, b-c) is in this way transformed into a new stationary state (Fig. 5.1,d).

The mathematical formulation of the stationary-state approximation is straightforward when a Lagrangian reference frame is adopted (*i.e.,* fixed with respect to a reference mass

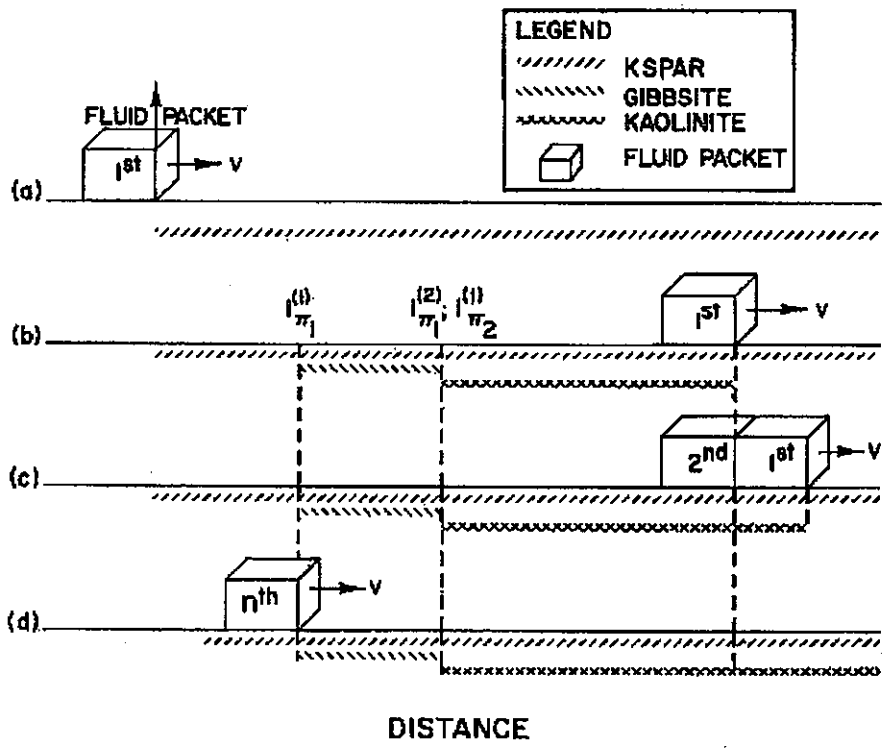

Figure 5.1.1_1. Schematic diagram illustrating the concept of stationary-states of an advective flow system resulting from coupled fluid flow and water-rock interaction (from Lichtner, 1988).

of fluid), and if constant one-dimensional advective fluid flow through a homogeneous porous medium is assumed. Under such conditions a stationary state of the system is represented by a set of first order ordinary differential equations (Lichtner, 1988):

$$v\frac{d\psi_j}{dx} = -\sum_r \nu_{j,r}\frac{\partial \Xi_r}{\partial t}(x;\{\phi_r\}), \tag{5.1.1.1}$$

where v stands for the Darcy fluid velocity, ψ_j (defined below) refers to the *generalized* concentration of the j-th primary species, x denotes the distance along the flowpath, $\nu_{j,r}$ represents a stoichiometric coefficient for the j-th primary species in a balanced chemical reaction involving dissolution or precipitation of the r-th mineral reacting at rate $\partial\Xi_r/\partial t$, and ϕ_r stands for the mineral's volume fraction (per unit volume of the porous medium). The generalized concentration is defined at a given position in the flowpath and time t by:

$$\psi_j(x,t) = C_j(x,t) + \sum_i \nu_{j,i}C_i(x,t), \tag{5.1.1.2}$$

where $C_j(x,t)$ represents the concentration of the j-th primary species and $\nu_{i,j}$ denotes a stoichiometric coefficient for the i-th secondary species, which is formed with concentration $C_i(x,t)$, in a balanced chemical reaction involving the j-th primary species. The reaction-rate, $\partial\Xi_r/\partial t$, refers to dissolution or precipitation of the r-th mineral. Assuming a general rate law for such reactions that is consistent with surface reaction control and transition state theory (see Section 4.1), it is given by (*e.g.*, Murphy and Helgeson, 1989):

$$\frac{\partial \Xi_r}{\partial t} = k_r s_r a_{H^+}^{n_{H^+}}\left[1-\exp(-A/\sigma RT)\right], \tag{5.1.1.3}$$

where k_r stands for the rate constant, s_r refers to the total surface area corresponding to a volume of the bulk porous medium containing a reference volume (*e.g.*, 1000 cm^3) of aqueous solution, n denotes the order of the reaction with respect to the activity (a) of the hydrogen ion, A represents the chemical affinity for the overall reaction, σ stands for the ratio of the rate of decomposition of the activated complex to that of the overall reaction (usually taken as being equal to one), R refers to the gas constant and T denotes temperature. The chemical affinity for the overall reaction is given by:

$$A = RT\ln(K_r/Q_r), \tag{5.1.1.4}$$

where K_r stands for the equilibrium constant and Q_r refers to the activity product for the overall reaction. Assuming $\sigma = 1$, Eqn. (5.1.1.3) can be rewritten as:

$$\frac{\partial \Xi_r}{\partial t} = k_r s_r a_{H^+}^{n_{H^+}}\left(1-\frac{Q_r}{K_r}\right), \tag{5.1.1.5}$$

where the logarithm of the quantity (Q_r/K_r) denotes the *saturation index*. Note that for far-from-equilibrium conditions, when $Q_r << K_r$, the reaction rate is given to a good approximation by:

$$\frac{\partial \Xi_r}{\partial t} = k_r s_r a_{H^+}^{n_{H^+}} . \qquad (5.1.1.6)$$

For the special case $n_{H+} = 0$, Eqn. (5.1.1.6) reduces to a linear rate law that is independent of solution composition.

For stationary-state conditions of constant porosity and Darcy flow velocity, the travel (or residence) time, t', of a fluid packet is related to distance along the flowpath, x, by:

$$x = \frac{vt'}{\phi}, \qquad (5.1.1.7)$$

where ϕ refers to porosity. This relation permits t' to be introduced as the independent variable in Eqn. (5.1.1.1):

$$\phi \frac{d\psi_j}{dt'} = -\sum_r \nu_{j,r} \frac{\partial \Xi}{\partial t}(t'; \{\phi_r\}) \qquad (5.1.1.8)$$

Equations (5.1.1.7) and (5.1.1.8) represent the Lagrangian formulation of the stationary-state approximation to coupled fluid flow and water-rock interaction. Equation (5.1.1.7) represents the equation of motion for the center of mass of a fluid packet, whose chemical composition is determined through Eqns. (5.1.1.8) by the residence time of the fluid in contact with the reacting minerals it encounters along the flowpath. Minerals that precipitate as a result of water-rock interaction are left behind as the fluid packet migrates downstream, and do not back react.

5.1.2 Modeling Approach

For a given stationary state, Eqns. (5.1.1.8) represent a conventional *reaction-path* model of water-rock interaction in an open system if it is assumed that absolute time in the reaction path is equivalent to the residence time of a packet of fluid traversing the flowpath (Lichtner, 1988). Solution of these equations yields the concentrations of aqueous species and mineral reaction rates as a function of absolute time. Taking this time to be equivalent to the residence time enables the temporal variations in solution composition and mineral reaction rates to be expressed as a function of location in the flowpath using Eqn. (5.1.1.7). This is important for the present study because it suggests that a kinetic reaction-path model can be used to solve for the residence time required for a given mineral to equilibrate with the aqueous phase, t_{eq}, and the corresponding location in the flowpath is given by Eqn. (5.1.1.7) assuming constant porosity and Darcy flow velocity. The distance between this location and a point in the flowpath upstream from it represents the characteristic length scale for equilibrium to be achieved, l_{eq}, if it is assumed that $t' = 0$ at $x = 0$, where x refers to the upstream point. If l_{eq} is less than or equal to the length of the flowpath considered in a groundwater evolution model, then the local equilibrium assumption is valid for reactions involving the minerals considered.

The reaction-path model was first described by Helgeson (1968), and is presently included in a number of geochemical software packages. Two such packages, EQ3/6 (Wolery,

1992) and the Geochemist's WorkBench (GWB; Bethke, 1996), also incorporate the rate law represented by Eqn. (5.1.1.3). The modeling approach can thus be implemented for the minerals comprising a given host rock using the kinetic data in Section 4 and Eqn. (5.1.1.3) in either EQ3/6 or GWB to solve Eqns. (5.1.1.8) for t_{eq}, from which l_{eq} can be calculated using Eqn. (5.1.1.7).

5.1.2.1 Benchmark of the approach

To evaluate the validity of the modeling approach we consider a problem solved by Lichtner (1988) involving the weathering of a porous granitic rock consisting initially of K-feldspar and quartz by infiltrating rainwater at 25°C. The conceptual model is similar to that illustrated in Fig. 5.1.1_1. The infiltrating solution is assumed to be out of equilibrium with respect to K-feldspar and quartz. As these minerals dissolve a sequence of alteration minerals precipitate in the order gibbsite - kaolinite – muscovite. The final solution is equilibrated with both muscovite and K-feldspar, and is supersaturated with respect to quartz due to its sluggish precipitation rate. Lichtner (*op. cit.*) assumes that the pH of the infiltrating solution becomes acidic (pH 4) prior to contact with the host rock by reactions in an overlying soil zone (not explicitly modeled). The initial volume fractions of K-feldspar and quartz are equal to 20 and 70%, respectively, and the corresponding surface areas are 12 and 40 $cm^2\ cm^{-3}_{rock}$. The infiltrating solution migrates through the host rock (porosity = 10%) with a Darcy flow velocity of 10 m yr^{-1}.

The modeling approach applied to this problem includes the following steps:

- simulation of the reaction path representing weathering of the granite;
- calculation of the time at which various minerals equilibrate with the solution; and
- transformation of these equilibration times (t_{eq}) to equilibration lengths (l_{eq}).

To simulate the reaction path representing granite weathering we use the open-system, reaction-path model in GWB and pH-independent apparent rate constants adopted by Lichtner (1988) for hydrolysis reactions involving K-feldspar ($k = 10^{-15.5}$ mol cm^{-2} sec^{-1}) and quartz ($k = 10^{-17.5}$ mol cm^{-2} sec^{-1}). The surface areas for K-feldspar and quartz are converted to values consistent with Eqn. (5.1.1.3) in GWB ($cm^2\ l^{-1}$) by dividing by the porosity and multiplying by a conversion factor of 1000 $cm^3\ l^{-1}$. Resultant values are 120,000 and 400,000 $cm^2\ l^{-1}$, respectively. Lichtner (*op. cit.*) assumes that the product of the apparent rate constants and surface areas of gibbsite, kaolinite and muscovite are sufficiently large that these phases closely approach local equilibrium with the aqueous phase when solution compositions evolve accordingly. Local equilibrium conditions for gibbsite, kaolinite and gibbsite, kaolinite and muscovite are simulated using GWB by assuming that the corresponding precipitation rates are instantaneous. Lichtner (1988) also accounts for variations in surface areas of K-feldspar and quartz using an empirical equation relating surface area to the volume fractions of these minerals. The surface area is assumed to be constant in calculations using GWB, however. Small differences in equilibrium constants for the relevant aqueous speciation and mineral hydrolysis reactions exist between the databases supporting our calculations and those carried out by Lichtner (*op. cit.*).

The results of the reaction-path simulation of granite weathering are shown in Fig. 5.1.2.1_1 by the bold curve on the *activity-activity* diagram for the K_2O-Al_2O_3-SiO_2-H_2O system. The reaction path advances along this curve from the lower left to the upper right. Gibbsite begins to precipitate at local equilibrium and continues to precipitate as both K-feldspar and quartz dissolve. Resultant variations in solution compositions then evolve to conditions where both gibbsite and kaolinite precipitate at local equilibrium (point *a*). Continued dissolution of K-feldspar and quartz extends the path into the kaolinite stability field, where gibbsite no longer precipitates. Quartz ceases to dissolve and begins to precipitate at the kinetically controlled rate when log $a_{SiO2(aq)} > -3.99$ (point *b*), near which point the reaction path takes an upward track and approaches local equilibrium of the aqueous phase with respect to both kaolinite and muscovite (point *c*). Continued dissolution of K-feldspar and precipitation of quartz extends the path into the stability field of muscovite, and it then approaches the stability boundary between muscovite and K-feldspar (point *d*). The path parallels this boundary as K-feldspar continues to dissolve at

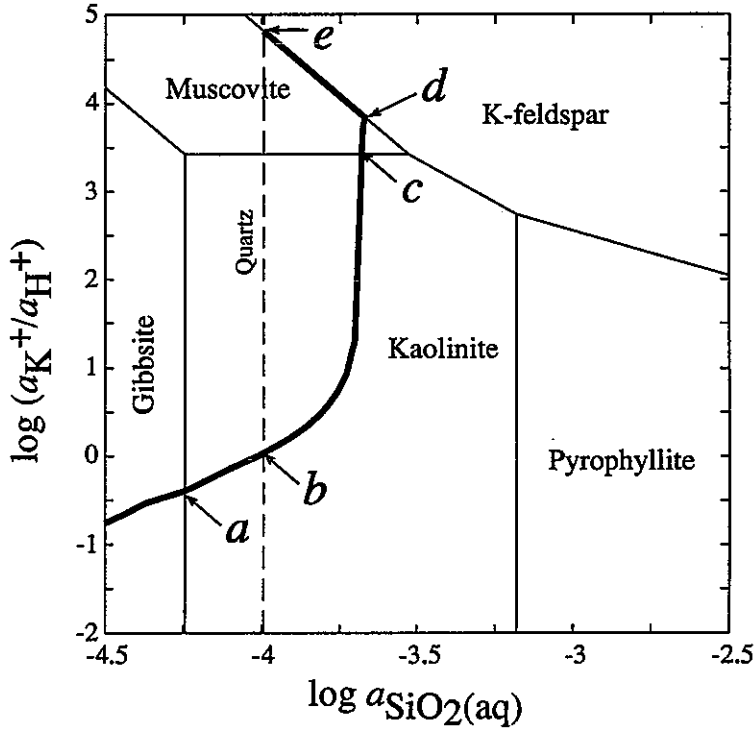

Figure 5.1.2.1_1: Reaction path (bold curve) representing weathering of a granitic rock consisting of K-feldspar and quartz at 25°C plotted on an *activity-activity* diagram for the system K_2O-Al_2O_3-SiO_2-H_2O.

an extremely low, close-to-equilibrium rate, and quartz continues to slowly precipitate. At the final stage of the reaction path *(e)*, K-feldspar is effectively equilibrated with the aqueous phase, as is muscovite, and the solution is very slightly supersaturated with respect to quartz.

The time evolution of the reaction path shown in Fig. 5.1.2.1_1 is represented in Fig. 5.1.2.1_2 in terms of the residence time (assumed to be equal to reaction-path time) and saturation indices for K-feldspar, quartz, gibbsite, kaolinite and muscovite. Labels *a-d* correspond to the events in the reaction path discussed above (the final increment of the

reaction path represented by the interval *d-e* in Fig. 5.1.2.1_1 is not shown in Fig. 5.1.2.1_2). Negative values of the saturation index indicate the solution is undersaturated with respect to the mineral, positive values indicate it is supersaturated, and local equilibrium is indicated when the saturation index equals 0. The point labeled *a*, for example, indicates that both gibbsite and kaolinite are equilibrated with the aqueous phase, because the saturation index for both minerals is equal to zero. With increasing time, the saturation index of gibbsite turns negative, indicating that it cannot precipitate, but the saturation index of kaolinite remains equal to zero up to about 0.085 years, at which time both muscovite and kaolinite are equilibrated with the solution. With regard to the primary minerals in granite, it can be seen that K-feldspar closely approaches equilibrium after about 0.125 years, but the solution remains supersaturated with respect to quartz at times exceeding 0.15 years.

The time evolution of the reaction path is transformed into spatial coordinates using Eqn. (5.1.1.7). It should be re-emphasized here that it is only necessary to calculate a single reaction path because each subsequent packet of fluid will trace out exactly the same reaction path as the first packet as long as stationary-state conditions of invariant porosity,

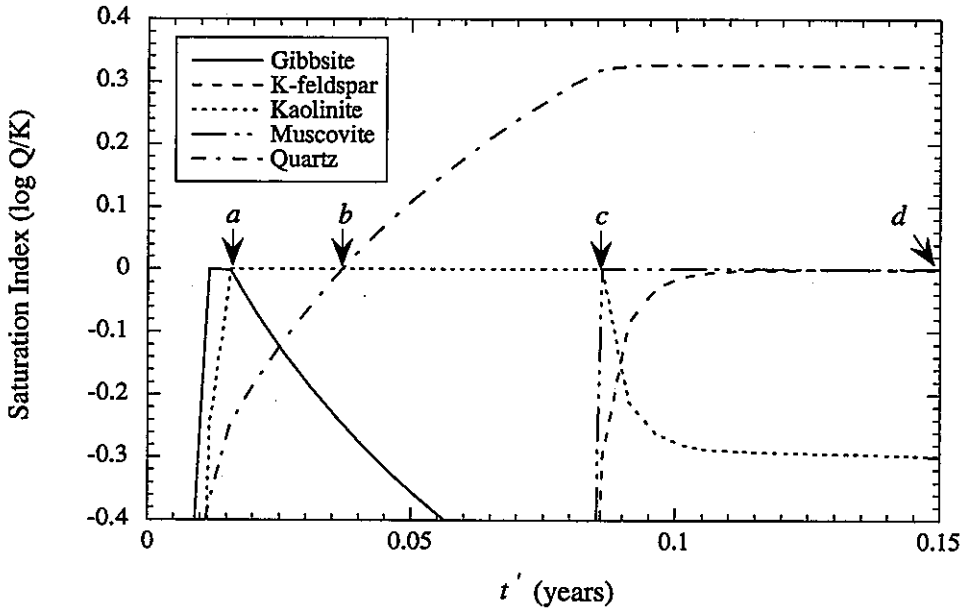

Figure 5.1.2.1_2: Saturation indices of reactant and product minerals associated with weathering of granite as a function of the residence time of infiltrating rainwater (see text).

mineral volume fractions, *etc.*, are approximately satisfied. The results of converting time in the calculated reaction path for granite weathering to spatial coordinates using Eqn. (5.1.1.7), with v/ϕ = 10 m yr^{-1} / 0.1 = 100 m yr^{-1}, are shown in Fig. 5.1.2.1_3. As can be seen, K-feldspar closely approaches equilibrium with the infiltrating rainwater about 12.5 m from the inlet. Taking x (Eqn. 5.1.1.7) = 0 m at the inlet, l_{eq} therefore equals 12.5 m. This indicates that the LEA would be a reasonable assumption for the K-feldspar hydrolysis reaction if the length scale of interest in the granite weathering problem is greater than 12.5 m. For example, assuming x = 0 at the soil-rock interface, and that the flow is advective and directed downward from this location, at depths in the weathering profile greater than 12.5 m from the soil-rock interface it is reasonable to assume that K-feldspar equilibrates

with a solution whose composition has evolved from rainwater by dissolution of K-feldspar and quartz, and by precipitation of gibbsite, then kaolinite and finally muscovite.

The results in Fig. 5.1.2.1_3 are closely consistent with those reported by Lichtner (1988). Equilibration lengths calculated by Lichtner (*op.cit*) for initial precipitation of gibbsite, kaolinite and muscovite are equivalent to those in Fig. 5.1.2.1_3, as near as can be determined by inspection of Fig. 8 in Lichtner (*op.cit*). Also in agreement are predictions that the evolved rainwater would become supersaturated with respect to quartz about 4 m from the soil-rock interface, and would closely approach equilibrium with K-feldspar about 12.5 m from this interface. The differences noted above between the modeling approach used here and that used by Lichtner (*op.cit*) do not significantly affect calculated results.

5.1.2.2 Practical constraints in using the modeling approach to estimate t_{eq} and l_{eq}

A number of practical constraints should be acknowledged when using the modeling approach described above to estimate equilibration times and lengths in real groundwater systems. Comments regarding several of these constraints are summarized below.

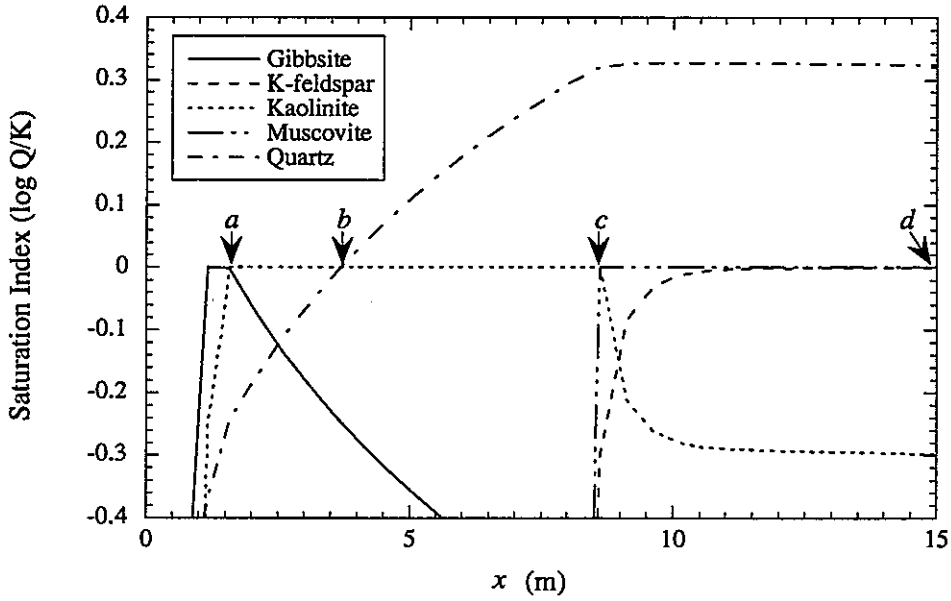

Figure 5.1.2.1_3: Saturation indices of reactant and product minerals associated with weathering of granite as a function of location in the flowpath (see text).

5.1.2.2.1 Conditional dependence of t_{eq} and l_{eq} on uncertainties in the saturation index

A necessary condition for equilibrium is that the reaction rate must be exactly equal to zero, which occurs when the saturation index (or chemical affinity) equals zero (see Section 5.1.1). There are uncertainties in any calculated value of the saturation index, however, which arise from uncertainties in thermodynamic data, in methods to analyze the chemical composition of groundwater samples and in techniques to estimate activity coefficients. To account for these uncertainties, a calculated value of the saturation index is generally taken to indicate equilibrium if it lies within a range of values centered upon zero. Wolery (1983), for example, estimates that if the saturation index equals 0.0±0.37, then it is reasonable to

assume equilibrium. Alternative estimates of the uncertainty in calculated values of the saturation index ranging between 0.0±0.1 and 0.0±1 may also be realistic (Wolery, *op. cit.*; Paces, 1972).

The estimated uncertainty in calculated values of the saturation index significantly affects estimates of t_{eq} and l_{eq}. This is because the rate law [Eqn. (5.1.1.3)] requires the rate to decelerate rapidly as equilibrium is more and more closely approached. The far-from-equilibrium rate [Eqn. (5.1.1.6)] is independent of solution composition (except possibly for pH), but near-to-equilibrium the ratio Q_r/K_r approaches unity, and the reaction rate must therefore approach zero. The transition from relatively fast reaction under far-from-equilibrium conditions to relatively slow reaction under near-to-equilibrium conditions occurs when the quantity

$$[1-(Q_r/K_r)]$$

in Eqn. (5.1.1.5) begins to decrease significantly from unity. Taking this to occur when the logarithm of the ratio Q_r/K_r is greater than about -2 implies that the transition from fast to slow reaction rates occurs near values of the saturation index that are comparable to the estimated uncertainty in this parameter (*e.g.*, 0.0±0.1 to 0.0±1, as noted above).

In practical terms this means that if reasonable uncertainties in calculated values of the saturation index are acknowledged, corresponding values of t_{eq} and l_{eq} must decrease significantly compared with values calculated assuming no uncertainty in this parameter. Although the time and corresponding length in the flowpath necessary to achieve "true" equilibrium in the sense that reaction rates are exactly equal to zero can be calculated using the modeling approach, these values are in effect meaningless given the uncertainties in calculating the saturation index. For example, values of l_{eq} for quartz and K-feldspar are defined when the respective curves for these minerals in Fig. 5.1.2.1_3 cross the boundaries of the diagram paralleling the x-axis, if it is assumed that the uncertainty in the saturation index for each mineral equals 0.0±0.4, represented by the range on the y-axis. Adopting a less-realistic and more restrictive range of uncertainties for the saturation index of these minerals of 0.0±0.001 significantly increases corresponding values of l_{eq} for K-feldspar (≈200 m), and especially for quartz (≈2500 m), as can be seen in Fig. 5.1.2.2.1_1.

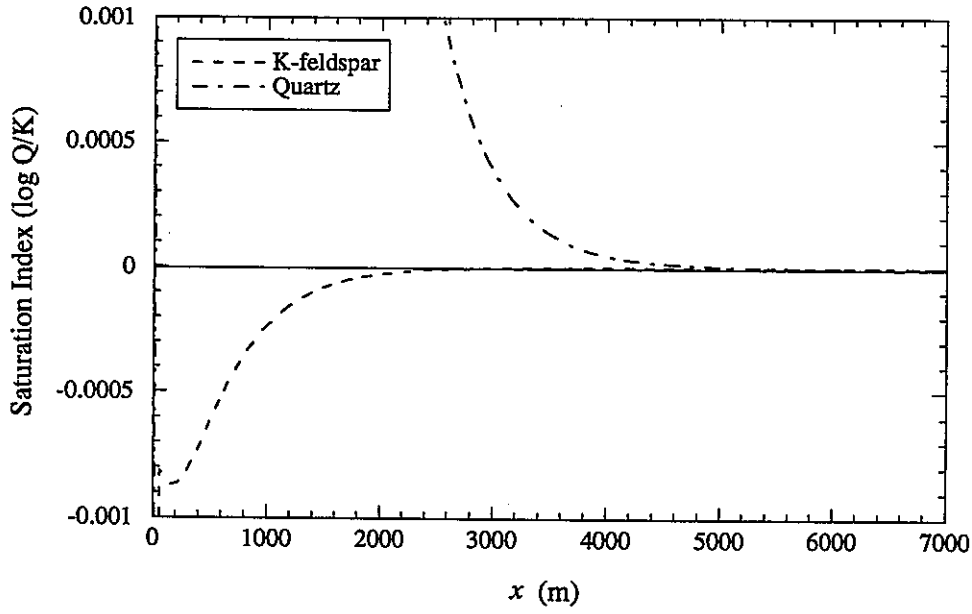

Figure 5.1.2.2.1_1: Saturation indices of K-feldspar and quartz considered in the granite weathering problem. Equilibration lengths are given by the intersection of the respective curves with the boundaries of the diagram that parallel the x-axis, assuming the uncertainty in corresponding saturation indices equals 0.0±0.001. Equilibration lengths for K-feldspar and quartz based on this assumption are considerably greater than predicted in Fig. 5.1.2.1_3, where it may be assumed that the uncertainty in the saturation index for these minerals equals 0.0±0.4.

Estimated values of t_{eq} and l_{eq} using the modeling approach described above are therefore conditional values because they depend on assumed uncertainties in the corresponding saturation index for each mineral evaluated. We assume in the following that this uncertainty is approximately equal to 0.0±0.4 for all mineral hydrolysis reactions, after Wolery (1983). Evaluations of the validity of the LEA using this modeling approach, or alternative approaches, should, however, set defensible limits on the uncertainty of the saturation index for each reaction considered.

5.1.2.2.2 Longevity of stationary-state conditions

It is assumed in the modeling approach that the duration of stationary-state conditions is greater than t_{eq}. The lifetime of a stationary state can be estimated by considering the time required to completely dissolve a reactant mineral at the inlet. This time is given by (Lichtner, 1988):

$$\tau_r = \frac{\phi_r}{\bar{V}_r k_r s_r}, \qquad (5.1.2.2.2.1)$$

where τ_r denotes the lifetime of the stationary state limited by complete dissolution of the r–th mineral and $\bar{v}_r$ stands for the molar volume. The denominator in this equation represents the time rate of change of the mineral's volume fraction assuming a linear rate law appropriate for far-from-equilibrium conditions. The longevity of the corresponding

stationary state will thus increase with increasing initial volume fraction and decreasing dissolution rate.

For conditions considered in the granite weathering problem, for example, and assuming that r refers to K-feldspar (molar volume = 108.74 cm^3 mol^{-1}; s_r = 12 $cm^2 cm^{-3}_{rock}$), $\tau_r \approx$16,000 years (this is a conservative estimate because a constant surface area is assumed). The stationary-state approximation is therefore appropriate for this problem because the duration of the stationary state is much longer than the time required for K-feldspar and all the other minerals in this system to equilibrate with infiltrating rainwater (Fig. 5.1.2.1_2). K-feldspar determines the duration of stationary-state conditions in this example because τ_r for quartz (molar volume = 22.688 cm^3 mol^{-1}; s_r = 40 $cm^2 cm^{-3}_{rock}$) is about 8 million years.

5.1.2.2.3 l_{eq} *vs characteristic length scales in groundwater evolution models*

An additional assumption in the modeling approach is that the mineralogy is homogeneous over a *characteristic length* of the flowpath that is equal to or greater than l_{eq}. This may be unrealistic in some cases because geologic systems typically exhibit considerable physical and mineralogical heterogeneity over spatial dimensions of a few meters or tens of meters (*e.g.*, Thompson and Jackson, 1996). An important aspect of any evaluation of the validity of the LEA in groundwater evolution models is therefore to assess whether it is reasonable to assume homogeneous conditions over a characteristic length of the flowpath (starting from the point where local equilibrium is to be assumed and extending upstream) that is at least equal to the equilibration length of the reaction, or reactions, in question. If this cannot be assumed, then the modeling approach in its present form is inappropriate. Although the modeling approach could be modified to account for mineralogical and other heterogeneities, we do not address these modifications in the present study.

5.1.2.2.4 Disparity between laboratory and field measurements of dissolution rates

Laboratory measurements of mineral dissolution rates are often found to be greater, by as much as several orders of magnitude, than rates estimated using a variety of techniques and data measured in the field (Paces, 1972, 1983; Velbel, 1985; White and Peterson, 1990). A number of reasons could explain such discrepancies, including:

- inhibition of the dissolution rate by the presence of an aqueous solute;
- a reduction in dissolution rate as equilibrium is closely approached; and
- underestimation of reactive surface area in the field.

Inaccurate estimates of the reactive surface area may be due in part to channeling of groundwater flow along preferential pathways, the effects of aging of reactant surfaces and formation of protective layers of secondary phases on mineral surfaces. As pointed out by Drever and Clow (1994), however, the number of investigations documenting the disparity between laboratory and field dissolution rates is extremely small, and it may therefore be premature to assume that the discrepancies are universal, or to attribute them to any single cause.
The modeling approach can accommodate the first two possible causes noted above using a suitable form of the rate law represented by Eqn. (5.1.1.3). The approach, however, must assume uniform advective flow through a homogeneous porous medium, and does not

presently account for the effects of aging of reactant surfaces or direct precipitation of product phases onto the surfaces of dissolving minerals. Equilibration times and lengths calculated using this approach could therefore underestimate t_{eq} and l_{eq} compared with actual values of these parameters in real groundwater systems. We note, however, that the surface area term in the rate equation [Eqn. (5.1.1.3)] may be treated as an adjustable parameter. The effects on calculated values of t_{eq} and l_{eq} associated with possible errors in estimating the reactive surface area in groundwater systems can therefore be approximated by adjusting the surface area downward accordingly.

5.2 Validity of the LEA in Geochemical Models of Groundwater Evolution at the Kamaishi Site

The technique summarized in Section 5.1 is evaluated below for reactions involving minerals in conductive fractures and fracture zones at the Kamaishi *in-situ* tests site. The objective of the evaluation is to estimate the time required for *all* the fracture minerals to equilibrate with a packet of groundwater as it passes through a single fracture. Based on this *global* equilibration time we estimate corresponding equilibration lengths using Eqn. (5.1.1.7), assuming a range of Darcy flow velocities between 0.01 and 10 m yr^{-1}, and a porosity of 10% for the fracture-fill material. This range is consistent with flow velocities observed in sedimentary basins and hydrothermal systems (Knapp, 1989), and measured flow velocities in fractured crystalline rocks (*e.g.*, at the Äspö Hard-Rock Laboratory in Sweden; see Wikberg *et al.*, 1991 and Rhén *et al.*, 1992).

5.2.1 Conceptual Model

The conceptual model illustrated in Fig. 5.1.1_1 is valid for a single fracture if it is assumed that the fracture-fill closely approximates a homogeneous porous medium, that groundwater flow is purely advective and that diffusion of solutes across the fracture-host rock boundary does not occur. Whether these assumptions are valid for conditions at the Kamaishi site is uncertain, but they are adopted here as a first approximation. Field investigations of fracture characteristics at the Kamaishi site are summarized by Sasamoto *et al.* (1993), Osawa *et al.* (1995) and Sasamoto *et al.* (1999b).

5.2.1.1 Fracture mineralogy

Fracture minerals in the Kurihashi granodiorite include, in order of decreasing abundance (Sasamoto *et al.*, 1993; Osawa *et al.*, 1995):

- calcite, stilbite > quartz, chlorite, laumontite > plagioclase, epidote > hornblende, sericite, prehnite.

Chlorite, epidote, hornblende and sericite (a fine-grained variety of muscovite, and possibly paragonite) are commonly associated with relatively high-temperature, high-pressure environments (Dana, 1949), and may be the remnants of an earlier hydrothermal event at the Kamaishi site (perhaps associated with development of the skarn-type Fe-Cu ore deposit mined at the site prior to 1993). We therefore assume that these minerals did not

form from dilute cold groundwaters similar to those presently circulating through fractures at the site, and exclude them from the conceptual model. Similarly, it is not known whether plagioclase precipitated from such groundwaters, or from an earlier hydrothermal solution. To account for the former possibility, we include plagioclase, as albite, in the conceptual model.

The fracture mineralogy in the conceptual model therefore includes:

- calcite, stilbite > quartz, laumontite > albite > prehnite.

Thermodynamic and kinetic data are unavailable for stilbite ($NaCa_2Al_5Si_{13}O_{36}\cdot 14H_2O$), and we therefore approximate its behavior by assuming these properties are identical with those of heulandite ($CaAl_2Si_7O_{18}\cdot 6H_2O$; *i.e.*, both phases are Ca-bearing monoclinic zeolites). Kinetic data are also unavailable for prehnite. We do not account for the dissolution rate of this phase, but assume that it precipitates instantaneously if solution compositions evolve accordingly. To account for the observed relative abundances of the fracture minerals, we assume volume fractions (*i.e.*, ϕ_r, see Section 5.1.1) equal to 30% for calcite and heulandite (representing stilbite), 15% for quartz and laumontite, and 10% for albite. The porosity is assumed to be 10%, as noted above.

5.2.1.2 Surface area

A rate law consistent with Eqn. (5.1.1.3) in GWB is used to calculate the dissolution and precipitation rates of calcite, heulandite (representing stilbite), quartz, laumontite and albite. The surface area, in units adopted in GWB for this rate law ($cm^2\ l^{-1}$), is calculated based on geometric considerations using:

$$s_r = \lambda a(\mathrm{r})\phi_r\left(\frac{1}{\phi}-1\right), \qquad (5.2.1.2.1)$$

where λ refers to a conversion factor equal to 1000 $cm^3\ l^{-1}$, $a(r)$ denotes the intrinsic surface area-to-volume ratio, which is a function of the radius, r, of individual grains, and other terms are as defined in Section 5.1.1. Grains of calcite and quartz are assumed to be spherical in shape [$a(r) = 3/r$], and those of heulandite, laumontite and albite are assumed to be cylindrical [$a(r) = 2/r$]. Assuming all the minerals are equidimensional with r = 0.1 cm, corresponding surface areas calculated using Eqn. (5.2.1.2.1) are:

- calcite; 81,000 $cm^2\ l^{-1}$
- heulandite; 54,000 $cm^2\ l^{-1}$
- quartz; 40,500 $cm^2\ l^{-1}$
- laumontite; 27,000 $cm^2\ l^{-1}$, and
- albite; 18,000 $cm^2\ l^{-1}$.

It is important to bear in mind that these values correspond to idealized geometries, which only approximate the actual intrinsic surface areas of these minerals. It is also implicit in the estimation technique that all surfaces are contacted by the aqueous phase. The technique does not account for surface roughness, which can significantly increase the true

reactive surface area (Murphy and Helgeson, 1989), nor does it account for similar increases or decreases in surface area resulting from reaction (*e.g.*, by formation of etch pits, or by dissolution, respectively). As noted in Section 5.1.2.2.4, however, the surface area may be treated as an adjustable parameter in Eqn. (5.1.1.3), and alternative estimates can therefore be accommodated in sensitivity analyses (Section 5.2.2.2).

5.2.1.3 Initial groundwater chemistry

The groundwater entering the fracture is assumed to be a dilute (0.0001 molal HCl) and mildly acidic (pH = 4) solution. To evaluate the effects on t_{eq} and l_{eq} of variations in initial groundwater compositions, we assume the carbonate content is fixed by the initial pH and either log P_{CO2} = -3.5 or log P_{CO2} = –2. The latter partial pressure could represent equilibration of the initial groundwater with soil gases, whereas the former value represents equilibration with the ambient atmosphere. Although the average groundwater temperature at the Kamaishi site is about 15°C (Sasamoto *et al.*, 1999b), a temperature of 25°C is assumed in the model for convenience (*i.e.*, to avoid the necessity of correcting thermodynamic and kinetic data for temperature effects). The higher temperature assumed in the model will accelerate dissolution rates slightly compared with values calculated at 15°C.

5.2.1.4 Kinetic and thermodynamic data

Rate constants and reaction orders for dissolution/precipitation reactions involving the fracture minerals are taken from relevant tables in Section 4. The selected values are:

- calcite; $k = 7.0 \times 10^{-11}$ mol cm^2 sec^{-1}, n_{H+} = 0 (Delany *et al.*, 1986)
- heulandite $k = 5.0 \times 10^{-19}$ mol cm^2 sec^{-1}, n_{H+} = -0.3 (Ragnarsdottir, 1993)
- quartz; $k = 1.6 \times 10^{-18}$ mol cm^2 sec^{-1}, n_{H+} = 0 (Murphy and Helgeson, 1989)
- laumontite; $k = 5.0 \times 10^{-17}$ mol cm^2 sec^{-1}, n_{H+} = 0 (Savage *et al.*, 1993), and
- albite; $k = 1.1 \times 10^{-14}$ mol cm^2 sec^{-1}, n_{OH-} = 0.3 (Chou and Wollast, 1985).

Trial calculations indicate that although the groundwater is initially acidic it quickly becomes alkaline as a result of the relatively rapid dissolution rate of calcite. Rate constants and reaction orders consistent with alkaline conditions are therefore adopted for heulandite and albite. The dissolution/precipitation rates of the other minerals are pH independent.

Thermodynamic data in the *thermo.dat* datafile supporting GWB are accepted at face value and used in the calculations. These data are extracted from the *data0.3245r46* database supporting EQ3/6, which was last modified in August, 1986.

5.2.1.5 Excluded phases

Trial calculations indicate that quartz and the zeolites heulandite and laumontite would not equilibrate with the evolved fracture groundwater unless it is assumed that tridymite and the Ca-end member of clinoptilolite solid solution are prevented from precipitating. Tridymite, a high-temperature polymorph of SiO_2, is unlikely to precipitate from aqueous solutions at low temperatures, and is therefore excluded from the model. Clinoptilolite is known to be stable under such conditions, but is not present in fractures at the Kamaishi

site. Ca-clinoptilolite is therefore also excluded from the model, possibly because the thermodynamic data for this phase are in error.

5.2.2 Reaction-Path Simulations

5.2.2.1 Nominal dissolution behavior

Reaction paths simulating the interaction of fracture minerals in the Kurihashi granodiorite with acidic groundwater are calculated using GWB and the input script shown in Table 5.2.2.1_1. This input file reflects nominal conditions in the conceptual model described above. Calculated variations in the saturation index of the fracture minerals as a function of time are shown in Fig. 5.2.2.1_1. Also shown, for reasons discussed below, are variations in the calculated saturation indices of chalcedony, gibbsite and kaolinite. Uncertainty in the saturation index for reactions involving all these minerals is assumed to be 0.0±0.4 (Section 5.1.2.2.1), and equilibrium is therefore assumed when the saturation indices plotted in the figure lie within this range.

As can be seen, all the fracture minerals equilibrate with the groundwater within 4 years in the "low P_{CO2}" reaction path (Fig. 5.2.2.1_1a), and within 5 years in the "high P_{CO2}" path (Fig. 5.2.2.1_1b). Equilibration times are determined by the dissolution rate of albite, because this mineral is the last to equilibrate with the evolved groundwater (as indicated by the intersection of the albite curves in Figs. 5.2.2.1_1a,b with the x-axis). The effect of increasing the initial carbonate concentration is to increase the global equilibration time slightly. Although prehnite no longer equilibrates with the groundwater after about 15 years in the high P_{CO2} path, this mineral is stable when albite first equilibrates with the groundwater. Both models are therefore consistent with the fracture mineralogy at the Kamaishi site for groundwater residence times of at least 30 years in the low-P_{CO2} path and less than about 15 years in the high-P_{CO2} path.

The saturation indices for chalcedony, gibbsite and kaolinite are included in Fig 5.2.2.1_1 because these minerals are *not* found in fractures at the Kamaishi site. *Realistic* equilibration times must therefore be consistent with two conditions: 1) equilibrium of the evolved groundwaters with respect to calcite, heulandite, quartz, laumontite, albite and prehnite, and 2) disequilibrium of these solutions with respect to chalcedony, gibbsite and kaolinite. Disequilibrium with respect to gibbsite occurs very early in both reaction paths (it is difficult to distinguish the calculated curves for gibbsite in Fig. 5.2.2.1_1a,b because they are virtually coincident with the y-axes). Kaolinite ceases to equilibrate with the evolved groundwater after about 5.4 years in the low-P_{CO2} path (Fig. 5.2.2.1_1a), and after about 8.7

```
# Groundwater evolution in fractures (Kamaishi)
data = thermo.dat
time start = 0 years, end = 30 years
temperature = 25
swap CO2(g) for HCO3-
1 kg free H2O
log fugacity CO2(g) = -2.
pH = 4
total molality Cl- = 0.0001
total molality Ca++ = 1.e-10
total molality Na+ = 1.e-10
total molality Al+++ = 1.e-10
```

```
total molality SiO2(aq) = 1.e-10
kinetic Calcite rate_con = 7.e-11 surface = 11.07
kinetic Quartz rate_con = 1.6e-18 surface = 11.33
kinetic Laumontite rate_con = 5.e-17 surface = 8.82
kinetic Albite rate_con = 1.1e-14 power(OH-) = 0.3
kinetic Albite surface = 7.65
kinetic Heulandite rate_con = 5.e-19 power(H+) = -0.3
kinetic Heulandite surface = 9.22
suppress  Tridymite Clinoptil-Ca
flow-through
porosity
delxi = 1e-4
dxprint = .01
react 7317 grams Calcite
react 5860 grams Heulandite
react 3575 grams Quartz
react 3060 grams Laumontite
react 2354 grams Albite
```

Table 5.2.2.1_1: Input script used with GWB to simulate the interaction of fracture minerals in the Kurihashi granodiorite with acidic groundwater. Note that the product of a mineral's mass with its specific surface area is equivalent to the surface area per liter of solution. The calculated porosity equals 10%.

years in the high-P_{CO2} path (Fig. 5.2.2.1_1b). Chalcedony remains equilibrated with the evolved groundwaters in both models for at least 30 years, however. This is because the difference in solubility between chalcedony and quartz is less than the uncertainty in the saturation index assumed here to indicate equilibrium, and because the rate of quartz precipitation is extremely low. Although a more restrictive range of uncertainties in the saturation indices for quartz and chalcedony may be reasonable, much longer periods of time would be required for the groundwater to equilibrate with quartz, and not with chalcedony (see Section 5.1.2.2.1). We therefore assume that all the fracture minerals, except quartz, equilibrate with the groundwater within 5.4 years (log P_{CO2} = -3.5) and 8.7 years (log P_{CO2} = -2), at which times both gibbsite and kaolinite are no longer stable. The apparent close approach to equilibrium of the groundwater with respect to chalcedony results from the similar solubilities of quartz and chalcedony, and the sluggish precipitation rate of quartz. This behavior is qualitatively consistent with the observation that only extremely old groundwaters closely approach, and perhaps achieve, equilibrium with respect to quartz (Rimstidt, 1997).

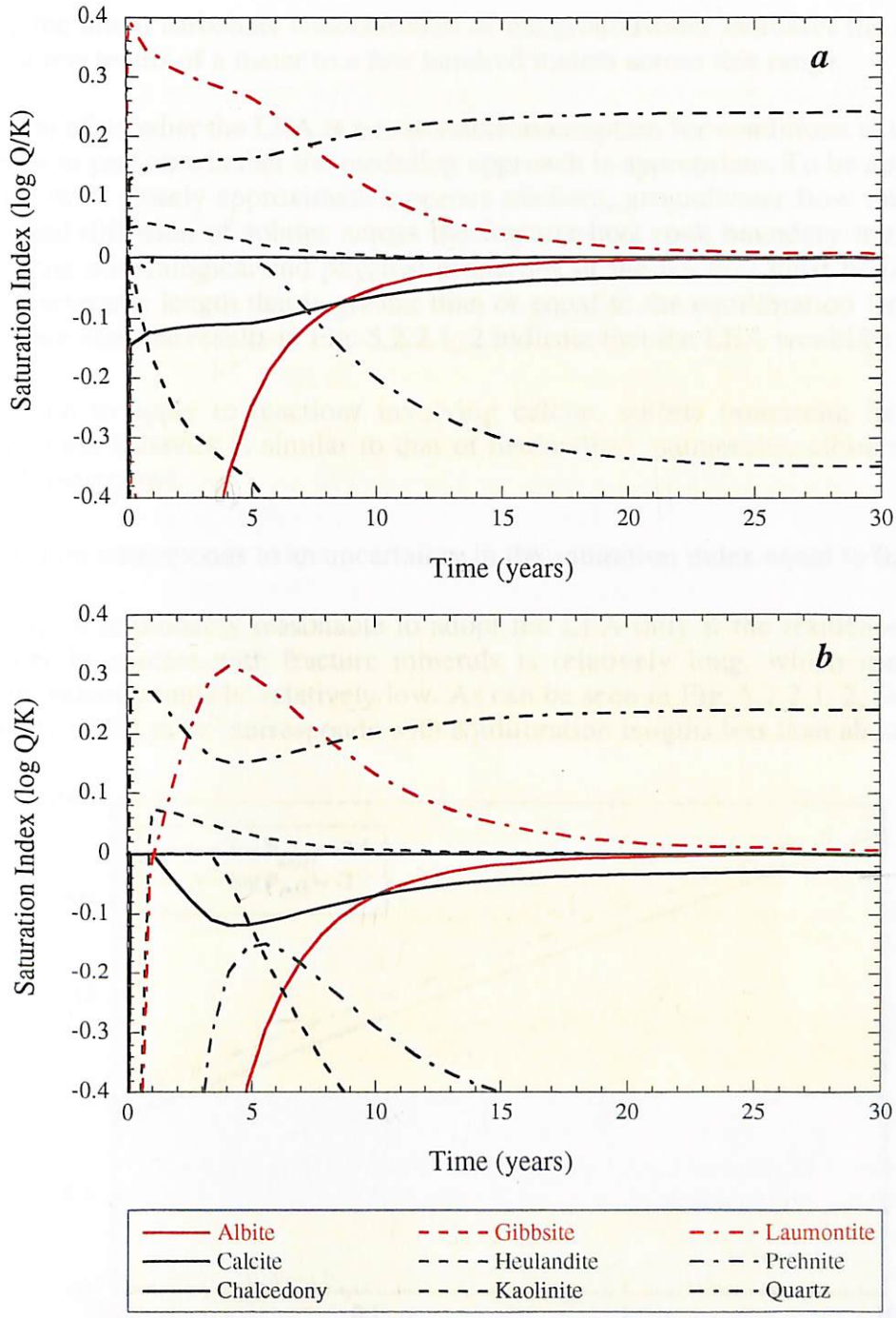

Figure 5.2.2.1_1: Calculated saturation indices as a function of time in the reaction path representing equilibration of fracture minerals in the Kurihashi granodiorite with dilute groundwater, where log P_{CO_2} = -3.5 *(a)*, or log P_{CO_2} = -2 *(b)*.

The realistic global equilibration times are transformed into equilibration lengths using Eqn. (5.1.1.7). Results are shown as a function of the Darcy flow velocity in Fig. 5.2.2.1_2, where the boundaries bracket the range of velocities observed in natural systems, as noted above. As can be seen, values of l_{eq} between 0.6 m and 900 m for the suite of fracture minerals at Kamaishi (excluding quartz) are consistent with this range of flow velocities.

Increasing the initial carbonate concentration of the groundwater increases the equilibration length by a few tenths of a meter to a few hundred meters across this range.

The question of whether the LEA is a reasonable assumption for conditions at the Kamaishi site depends in part on whether the modeling approach is appropriate. To be appropriate the fracture fill must closely approximate a porous medium, groundwater flow must be purely advective and diffusion of solutes across the fracture-host rock boundary must not occur. Moreover, the mineralogical and physical properties of the fracture must be homogeneous over a characteristic length that is greater than or equal to the equilibration length. If these conditions are met, the results in Fig. 5.2.2.1_2 indicate that the LEA would be valid if:

- it is taken to apply to reactions involving calcite, stilbite (assuming its dissolution/ precipitation behavior is similar to that of heulandite), laumontite, albite and prehnite, but not quartz, and

- equilibrium corresponds to an uncertainty in the saturation index equal to 0.0±0.4.

Realistically, it is probably reasonable to adopt the LEA only if the residence time of the groundwater in contact with fracture minerals is relatively long, which means that the Darcy flow velocity must be relatively low. As can be seen in Fig. 5.2.2.1_2, for example, a flow velocity of 0.1 m yr^{-1} corresponds with equilibration lengths less than about 10 m, and

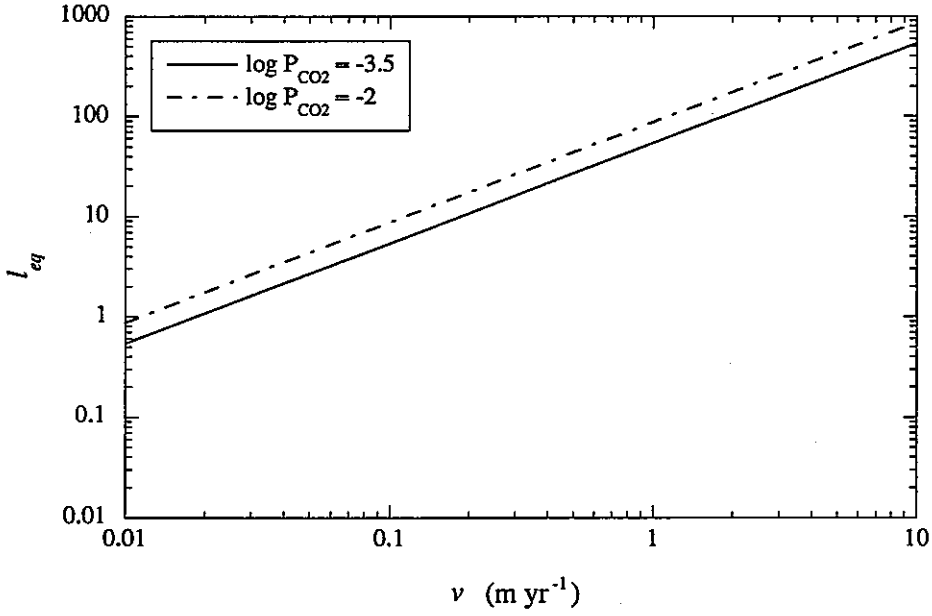

Figure 5.2.2.1_2: Equilibration lengths plotted as a function of the Darcy flow velocity for interaction of fracture minerals at the Kamaishi site with infiltrating rainwater.

it may be realistic to assume that fracture properties are homogeneous over this length scale. On the other hand, if a flow velocity of 10 m yr^{-1} is assumed, fracture properties would have to be homogeneous over a characteristic length between 400 and 900 m (depending on the initial carbonate concentration of the groundwater), which is almost certainly unrealistic.

5.2.2.2 Field *vs.* laboratory dissolution rates

In this section we consider the possibility that dissolution rates under field conditions at the Kamaishi site are less than predicted under nominal conditions, possibly because the estimated surface areas (Section 5.2.1.2) are in error for reasons discussed in Section 5.1.2.2.4. We assume, for example, that the dissolution/precipitation rates of calcite, heulandite, quartz, laumontite and albite are all 100 times smaller than predicted under nominal conditions. Resulting reaction paths for the low-P_{CO2} and high-P_{CO2} models are shown in Fig. 5.2.2.2_1, where temporal variations in the saturation index of the fracture minerals and gibbsite, kaolinite and chalcedony are plotted, and where it is assumed that equilibrium is indicated if the saturation index lies in the range 0.0±0.4.

As can be seen, temporal variations in the calculated saturation indices are similar to those shown in Fig. 5.2.2.1_1, but the curves span a period 100 times longer than predicted under nominal conditions. Associated effects on equilibration lengths are shown in Fig. 5.2.2.2_2, where it can be seen by comparison with Fig. 5.2.2.1_2 that l_{eq} increases uniformly by a factor of 100 over the same range of Darcy flow velocities. A reduction in reaction rate thus results in a proportional increase in l_{eq}. The modeling approach may be inappropriate for assessing the validity of the LEA over most of the conditions considered in this example, because it is probably unrealistic to assume that the fracture mineralogy is homogeneous over characteristic lengths greater than a few meters to tens of meters (Section 5.1.2.2.3).

5.2.3 Summary

The LEA is a reasonable assumption in geochemical models of groundwater evolution at the Kamaishi site, if conditions in the conceptual model summarized in Section 5.2.1 are valid, and if:

- the LEA applies to reactions involving calcite, stilbite (assuming its dissolution/ precipitation behavior is similar to that of heulandite), laumontite, albite and prehnite, but not quartz;
- Darcy velocities are relatively low (*e.g.*, less than about 0.1 m yr^{-1}, in which case the characteristic length is less than about 10 m); and
- equilibrium corresponds with an uncertainty in the saturation index equal to 0.0±0.4.

If, however, reaction rates are less than predicted in the conceptual model, possibly for reasons summarized in Section 5.1.2.2.4, the modeling approach may be inappropriate for

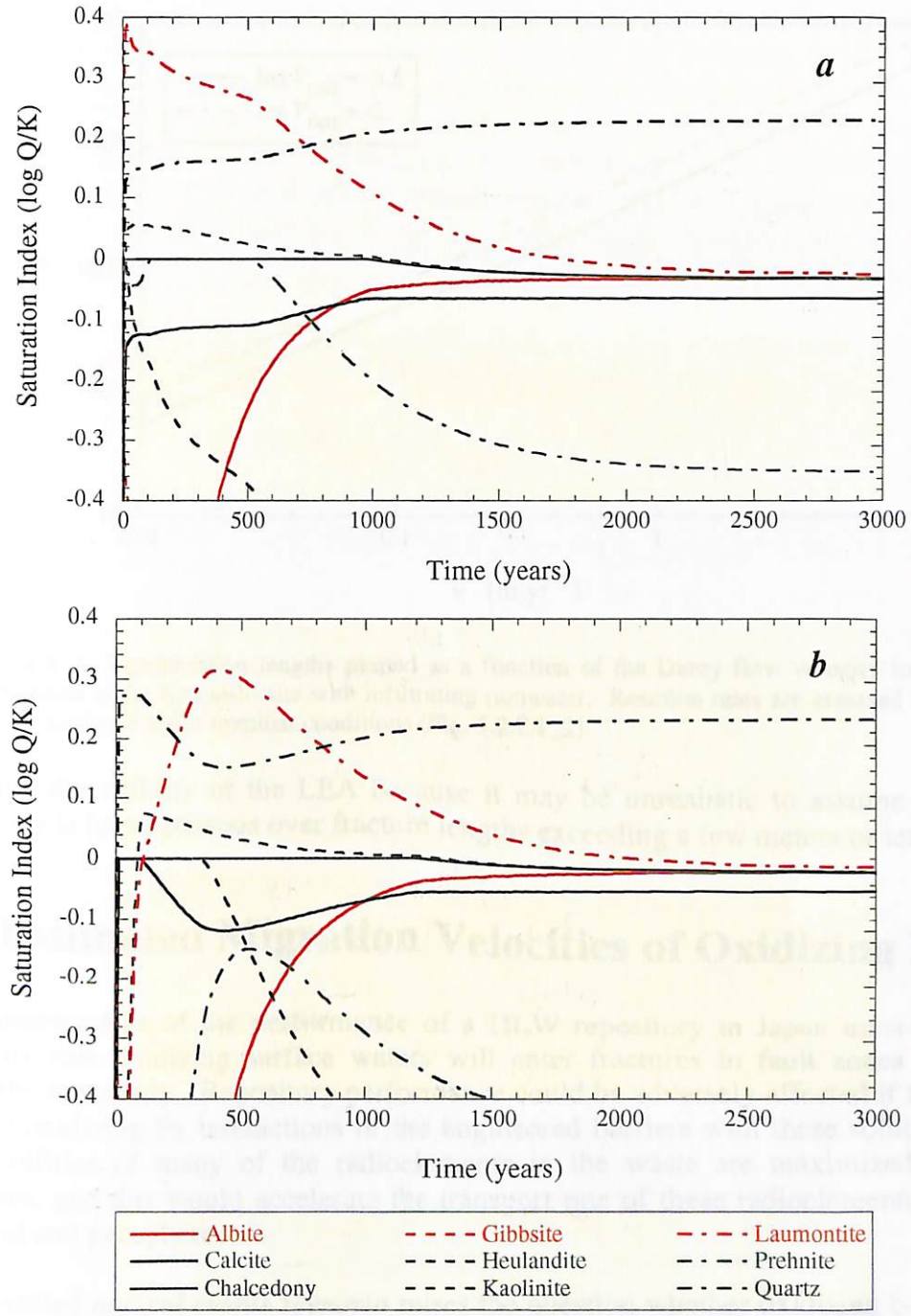

Figure 5.2.2.2_1: Calculated saturation indices as a function of time in the reaction path representing equilibration of fracture minerals in the Kurihashi granodiorite with dilute groundwater, where log P_{CO2} = -3.5 *(a)*, or log P_{CO2} = -2 *(b)*. The dissolution rates of albite, calcite, heulandite, laumontite and quartz are assumed to be two orders of magnitude smaller than nominal values (Fig. 5.2.2.1_1).

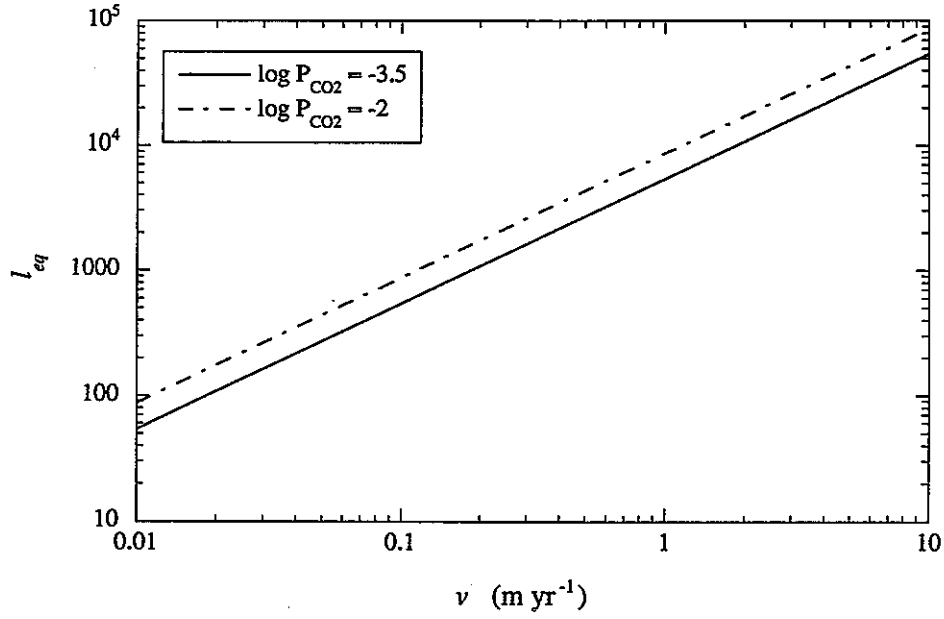

Figure 5.2.2.2_2: Equilibration lengths plotted as a function of the Darcy flow velocity for interaction of fracture minerals at the Kamaishi site with infiltrating rainwater. Reaction rates are assumed to be 100 times lower than considered under nominal conditions (Fig. 5.2.2.1_2).

evaluating the validity of the LEA because it may be unrealistic to assume that fracture mineralogy is homogeneous over fracture lengths exceeding a few meters or tens of meters.

5.3 Estimated Migration Velocities of Oxidizing Fronts

Safety assessments of the performance of a HLW repository in Japan must consider the possibility that oxidizing surface waters will enter fractures in fault zones and migrate toward the repository. Repository performance could be adversely affected if the near-field becomes oxidizing by interactions of the engineered barriers with these solutions because the solubilities of many of the radioelements in the waste are maximized under such conditions, and this would accelerate the transport rate of these radioelements through the near-field and geosphere.

This so-called *natural events scenario* raises the question whether oxidizing conditions can be propagated to repository depths over time scales that are relevant to repository performance. To address this question, JNC has developed a conceptual model of surface water migration through vertically oriented fractures in a fault zone 3 m in width, 700 m in length and at least 1000 m deep. The hydraulic conductivity of the fractures is assumed to be 3.15 x 10^3 m yr^{-1}, and the hydraulic gradient is assumed to be in the range 0.05 to 0.3. The corresponding range of Darcy flow velocities is between 158 to 945 m yr^{-1}. Assuming the repository is located 1000 m below the surface, as is envisaged for a repository in crystalline rock, the minimum time for oxidizing surface waters to reach repository depths is thus between 1.1 and 6.3 years.

These estimated times are almost certainly too short, however, because heterogeneous oxidation-reduction reactions are not accounted for. In JNC's conceptual model, pyrite, Fe(II)-silicates and organic carbon are assumed to exist in the fault zone. Dissolution of these minerals and organic carbon, and aqueous oxidation of Fe(II) and C(0) to Fe(III) and C(VI), would lower oxidant concentrations in the groundwater. The propagation velocity of the resulting *redox front* would be retarded relative to the fluid-flow velocity by an amount that depends on mass-balance, mass-action and kinetic constraints among all the oxidation-reduction reactions involved.

In this section we estimate redox-front migration velocities using an analytical model consistent with the stationary-state approximation and conditions in JNC's conceptual model. The model is briefly summarized in Section 5.3.1, and is derived in the appendix. Redox-front velocities are estimated in Section 5.3.3 using conceptual model constraints summarized in Section 5.3.2.

5.3.1 Analytical Model of Redox-Front Migration

An important consequence of stationary-state behavior is that the rate at which reaction fronts are propagated is fixed relative to the Darcy flow velocity. The migration velocity of a redox front, or any other reaction front, is given by:

$$v_f = \frac{v}{\phi(1+L_j)}, \tag{5.3.1.1}$$

(Lichtner, 1988; see appendix) where v_f stands for the velocity of the front (m yr^{-1}) and other terms are as defined in Section 5.1.1. The parameter, L_j, is a dimensionless quantity for the j-th aqueous reactant:

$$L_j = \frac{\sum_{r=1}^{M}\left(\frac{\nu_{j,r}}{\bar{V}_r}\right)\{\phi_r\}}{\phi\{\psi_j\}}, \tag{5.3.1.2}$$

where M refers to the number of minerals, r, that react with j, $\nu_{j,r}$ represents the stoichiometric coefficient for j in a balanced dissolution reaction (which may include oxidation/reduction) involving the r-th mineral, $\bar{V}_r$ stands for the molar volume (cm^3 mol^{-1}), and $\{\phi_r\}$ and $\{\psi_j\}$ denote differences in the volume fraction of the r-th mineral and generalized concentration of the j-th reactant, respectively, as measured between upstream and downstream points on either side of the reaction front.

The migration velocity of a redox front is retarded relative to the fluid velocity when $L_j > 0$. Moreover, if $L_j >> 1$, the front's velocity is independent of porosity and Eqn. (5.3.1.1) can be rewritten as:

$$v_f = \frac{v\{\psi_j\}}{\sum_{r=1}^{M}\left(\frac{\nu_{j,r}}{\overline{V}_r}\right)\{\phi_r\}}. \qquad (5.3.1.3)$$

The front velocity is thus proportional to $\{\psi_j\}$, and inversely proportional to the volumetric concentrations of reactant minerals. The front is stationary until ϕ_r is reduced significantly, at which time a new stationary state is generated and the front advances.

The absence of kinetic parameters in Eqn. (5.3.1.3) suggests that equilibrium is assumed in this application of the stationary-state approximation, but reaction rates are in fact considered explicitly. These rates determine both the position of the front in a given stationary state and also the time required to generate the next stationary state. Because the front velocity is given by the ratio of this distance and time, however, kinetic factors cancel and the front propagates at a constant velocity that is reaction-rate independent (Ortoleva *et al.*, 1986; Lichtner, 1988). Kinetically controlled heterogeneous reactions may initially delay generation of a reaction front, but once formed the front is propagated at a constant velocity equal to that which would occur under conditions of instantaneous reaction and local equilibrium. This is important because kinetic data for many oxidation-reduction and mineral-dissolution reactions are either lacking or are highly uncertain (Section 4). Additional uncertainty in quantifying the reactive surface area of minerals (and porosity) in natural systems (Section 5.1.2.2.4) further underscores the advantages of this modeling approach.

5.3.1.1 Previous applications of the model

Lichtner and Waber (1992) use the analytical model described above to estimate the velocity of redox fronts associated with pyrite oxidation in host rocks of the Osamu Utsumi uranium mine at Pocos de Caldas, Brazil. The following reaction is assumed to be rate limiting,

$$FeS_2 + H_2O(l) + 7/2\ O_2(aq) \rightarrow Fe^{2+} + 2SO_4^{2-} + 2H^+,$$

and the migration velocity of the corresponding front is calculated using Eqn. (5.3.1.3):

$$v_f = \frac{v\{\psi_{O_2(aq)}\}}{\nu_{O_2(aq),py}\{\phi_{py}\}\overline{V}_{py}^{-1}}. \qquad (5.3.1.1.1)$$

Assuming that the concentration of dissolved oxygen is approximately equal to zero immediately downstream of the front, and that $\phi_{py} = 0$ in previously oxidized regions upstream of the front:

$$\{\psi_{O_2(aq)}\} \approx \psi_{O_2(aq)}(x = 0, t' = 0) = K_H^{-1} P_{O_2(g)}, \text{ and}$$

$$\{\phi_{py}\} = \phi_{py}^0,$$

where K_H denotes the Henry's law constant for the reaction $O_2(aq) \leftrightarrow O_2(g)$, $P_{O2(g)}$ represents the partial pressure of $O_2(g)$ and ϕ^0_{py} refers to the volume fraction of pyrite in unoxidized host rocks (note that if, as here, K_H is in units of bar $-(\text{mol } l^{-1})^{-1}$, it is necessary for consistency among units to multiply the numerator in Eqn. (5.3.1.1.1) by a conversion factor, 0.001 l cm^{-3}, if the molar volume is in units of cm^3 mol^{-1}).

Lichtner and Waber (1992) assume $P_{O2(g)} = 0.2$ bar, $v = 1$ m yr^{-1}, $K_H = 10^{2.899}$ (at 25°C) and $\phi^0_{py} = 2\%$ (consistent with field data at the Pocos de Caldas site). With $\nu_{O2(aq),py} = 3.5$, based on reaction stoichiometry, and $\bar{v}_{py} = 23.99$ cm^3 mol^{-1}, the calculated velocity of the redox front equals 8.6 x 10^{-5} m yr^{-1}. This estimate slightly exceeds estimates based on natural series radionuclide profiles, which suggest that maximum front velocities are about 1 x 10^{-5} m yr^{-1} (MacKenzie *et al.*, 1991). The higher velocity predicted by the analytical model is consistent with the observation that diffusion, rather than pure advection, may be an important transport mechanism in the near vicinity of the front (MacKenzie *et al.*, 1991). Diffusion (including matrix diffusion) would spread an oxidizing front over larger volumes of host rock compared with advection-dominated systems, which would slow the front's migration velocity in the direction of flow. The analytical model therefore appears to yield approximate, yet conservative, estimates of front velocities at Pocos de Caldas.

Arthur (1996) used the analytical model described above to estimate the time required for an oxidizing front to migrate 500 m in granitic rock, which are the depth and rock type considered in the Swedish KBS-3 concept for disposal of spent nuclear fuel. Results indicate that small amounts of ferrous minerals in the granite matrix and fractures would strongly retard the downward migration of oxidizing conditions, which could be generated by infiltration of glacial meltwaters during periods of glacial maxima and retreat. Calculated front velocities are retarded relative to Darcy fluxes by factors ranging from 10^{-3} to 10^{-4}. Corresponding times required for the front to migrate from the surface to the repository vary between 5,100 and 4,400,000 years, assuming fluid-flow velocities between 30 and 0.3 m yr^{-1}, respectively.

5.3.2 Conceptual Model

JNC's conceptual model of oxidizing groundwaters migrating through a fracture is consistent with the stationary-state model illustrated in Fig. 5.1.1_1, if it is assumed that the fracture-fill closely approximates a homogeneous porous medium, that groundwater flow is purely advective and that diffusion of solutes across the fracture-host rock boundary does not occur. We also assume that the infiltrating groundwater is a dilute solution and that $O_2(aq)$ is the only oxidant species initially present. The initial solution is equilibrated with air ($P_{O2(g)} = 10^{-0.68}$ bar) at 0°C [$K_H = 10^{2.66}$ bar $-(\text{mol } l^{-1})^{-1}$]. The low temperature conservatively maximizes $O_2(aq)$ concentration ($10^{-3.34}$ mol l^{-1}) because the Henry's law constant for the reaction $O_2(aq) \leftrightarrow O_2(g)$ is minimized at this temperature. Because dissolved oxygen is consumed at the redox front by reactions involving organic carbon, pyrite and Fe(II) silicates, the concentration of $O_2(aq)$ in solutions immediately downstream of the front is low and $\{\psi_{O2(aq)}\} \approx 10^{-3.34}$ mol l^{-1}.

5.3.2.1 Redox reactions

The conceptual model assumes that pyrite, organic carbon and an Fe(II) silicate exist initially in the fracture fill. Stoichiometric and molar volume data for the corresponding reactions are summarized in Table 5.3.2.1_1, where stoichiometric coefficients, $\nu_{O2(aq),r}$, refer to reactions involving fully oxidized solutions in which redox-sensitive species exist in their highest oxidation state, and assuming that chlorite (*var.* daphnite) is generally representative of reactions involving ferrous silicates.

5.3.2.2 Initial concentrations of reactants

In JNC's conceptual model it is assumed that pyrite, ferrous silicate and organic carbon comprise the following mass fractions, x_r, (in weight %) of the fracture fill:

- pyrite; 0.1 – 1,
- Fe(II) silicate; 0.1 – 10, and
- organic C; 0.1 – 2.

The following equation is used to convert these concentrations into volume fractions, ϕ_r:

$$\phi_r = \frac{x_r \rho_f \overline{V}_r}{W_r}, \qquad (5.3.2.2.1)$$

where ρ_f stands for the density of the fracture fill, and W_r refers to molecular weight. The volume fractions of pyrite, chlorite (representing ferrous silicate) and organic carbon calculated using this equation, the molar volume data in Table 5.3.2.1_1, molecular weights of pyrite, chlorite and organic carbon equal to 119.967, 713.507 and 30.03 g mol^{-1}, respectively, and a density of the fracture fill equal to 2.7 g cm^{-3} are:

Mineral	Reaction	$\nu_{O2(aq),r}$	$\overline{V}_r$ (cm^3 mol^{-1})
pyrite [FeS_2]	pyrite + $15/4O_2(aq)$ + $1/2H_2O(l) \leftrightarrow Fe^{3+} + H^+ + 2SO_4^{2-}$	3.75	23.94[a]
chlorite (daphnite) [$Fe_5Al_2Si_3O_{10}(OH)_8$]	chlorite + $21H^+ + 5/4O_2(aq) \leftrightarrow 2Al^{3+} + 3SiO_2(aq) + 5Fe^{3+} + 29/2H_2O(l)$	1.25	213.4[a]
organic carbon [CH_2O]	$CH_2O + O_2(aq) \leftrightarrow HCO_3^- + H^+$	1.00	36.85[b]

[a] Arthur *et al.* (1999); [b] computed using the density and molecular weight of formaldehyde (CH_2O) from Weast (1979).

Table 5.3.2.1_1: Stoichiometric and molar volume data for minerals considered in the conceptual model of redox-front migration in fractures at the Kamaishi site.

ϕ_{pyrite}; 0.00054 – 0.0054
$\phi_{chlorite}$; 0.00081 – 0.081, and
$\phi_{org.C}$; 0.0033 – 0.066.

The molecular weight and molar volume data for pyrite and chlorite are from the SUPCRT thermodynamic database (*e.g.*, Arthur *et al.*, 1999). Molecular weight and molar volume

data for organic carbon are approximated using the data for formaldehyde (CH_2O) from Weast (1979). The density of the fracture fill is assumed to be similar to that of a highly compacted fine-grained sediment (Davis and DeWiest, 1966).

5.3.3 Estimated Redox-Front Velocities

The analytical model of redox-front velocities [Eqn. (5.3.1.3)] and data representing the conceptual model described in Section 5.3.2 are used in this section to calculate front retardation factors, v_f/v, and times required for oxidizing conditions to migrate 1000 m. The retardation factors indicate the relative efficiency of reactions involving pyrite, chlorite and organic carbon in retarding the migration velocity of a redox front relative to that of the fluid phase. The time required for the front to migrate 1000 m represents the minimum time required for oxidizing conditions to reach a HLW repository in Japan, assuming groundwater flows in a vertical fracture extending from the surface to repository depths. These *travel time* calculations are carried out for two cases: 1) *weak redox buffering* associated with minimal initial concentrations (*i.e.* ,ϕ_r) of pyrite, chlorite and organic carbon, and 2) *strong redox buffering* associated the maximum initial concentrations of these reactants.

5.3.3.1 Front retardation factors

Front retardation factors for a given redox reaction are derived by dividing the right- and left-hand sides of Eqn. (5.3.1.3) by the Darcy flow velocity, v, for the case $M = 1$. Results, using $\nu_{O2(aq),r}$ and $\bar{v}_r$ from Table 5.3.2.1_1, are:

pyrite; $v_f/v = 0.006\{\psi_{O2(aq)}\}/\{\phi_{pyrite}\}$,
chlorite; $v_f/v = 0.171\{\psi_{O2(aq)}\}/\{\phi_{chlorite}\}$, and
organic carbon; $v_f/v = 0.037\{\psi_{O2(aq)}\}/\{\phi_{org.C}\}$,

where, because units for $\psi_{O2(aq)}$ are in mol l^{-1}, the right-hand side of Eqn. (5.3.1.3) is multiplied by a conversion factor, 0.001 l cm^{-3}, to maintain consistency among units. For equivalent initial volume fractions of pyrite, chlorite and organic carbon, the efficiency of the corresponding reactions in retarding the migration velocity of an oxidizing front relative to that of the fluid decreases in the order pyrite > organic carbon > chlorite.

5.3.3.2 Travel time estimates for oxidizing fronts to migrate 1000 m

Minimum travel times for an oxidizing front to migrate in a vertical fracture extending from the surface to a repository located 1000 m below the surface are calculated by dividing this distance by the front's velocity. Using values of the parameters in Eqn. (5.3.1.3) from Table 5.3.2.1_1, values of ϕ_r from Section 5.3.2.2 for both *weak* (minimum values of ϕ_r) and *strong* (maximum values of ϕ_r) redox buffering, and assuming $\{\psi_{O2(aq)}\} = 10^{-3.34}$ mol l^{-1}, the calculated front velocities are:

$v_{f,weak} = 2.6 \times 10^{-3} v$, and
$v_{f,strong} = 1.5 \times 10^{-4} v$,

or,

$v_{f.weak}$ = 0.41 – 2.5 m yr^{-1}, and
$v_{f.strong}$ = 0.02 - 0.14 m yr^{-1},

assuming Darcy flow velocities between 158 – 954 m yr^{-1} (see above). Corresponding travel times are:

t_{weak} = 2,439 – 400 years, and
t_{strong} = 50,000 – 7,143 years.

The longest travel time results from strong redox buffering and low groundwater flow, whereas the shortest travel time results from weak redox buffering and fast groundwater flow.

5.3.4 Summary

An analytical model of redox-front migration behavior based on the stationary-state approximation to coupled fluid flow and water-rock interaction, and JNC's conceptual model of the migration of oxidizing surface waters in fractures, suggests that oxidizing solutions could travel from the surface to repository depths within 400 to 50,000 years. This broad range of calculated travel times is consistent with estimated Darcy flow velocities between 158 and 954 m yr^{-1}, and ranges in the concentrations of pyrite, Fe(II)-silicate (represented by chlorite) and organic carbon in fracture fill between 0.1 – 1, 0.1 – 10 and 0.1 – 2 wt.%, respectively. Calculated front velocities are retarded relative to fluid-flow velocities by factors ranging from 2.6 x 10^{-3} to 1.5 x 10^{-4} under these conditions.

The travel-time estimates noted above are relatively short compared with time periods considered in safety assessments of repository performance, which suggests that time-dependent variations in the redox environment of both the near field and geosphere may need to be accounted for in these assessments. We note, however, that the range of Darcy flow velocities and concentrations of reducing minerals in the fracture fill are probably conservative estimates in JNC's conceptual model. Front velocities would be more strongly attenuated than predicted here if lower (and perhaps more realistic) flow rates, and higher concentrations of reducing minerals in fractures, are assumed. Similar estimates for granitic rocks in Sweden, for example, suggest that travel times over a distance of 500 m would be between about 5,000 to 4,000,000 years (Arthur, 1996). In these calculations Darcy fluxes between 0.3 and 30 m yr^{-1} were assumed and concentrations of pyrite and chlorite in fractures were estimated to be equal to 0.2 and 35 vol.%, respectively.

6 Summary and Conclusions

Kinetic data, including rate constants, reaction orders and activation energies, are compiled in this report for 34 hydrolysis reactions involving feldspars, sheet silicates, zeolites, oxides, pyroxenes and amphiboles, and for similar reactions involving calcite and pyrite. The data are compatible with a rate law consistent with surface reaction control and transition-state theory, which is incorporated in the geochemical software packages EQ3/6 and GWB. The data are compiled from the results of previous investigations, in which empirical rate laws are used to retrieve values of corresponding rate constants and reaction orders from critically evaluated experimental data. The transition-state rate law is mathematically equivalent to the empirical rate laws under far-from-equilibrium conditions, however. Kinetic parameters determined in the retrieval studies may therefore be used under these conditions in calculations using EQ3/6 or GWB. The data may be conceptually consistent with the transition-state rate law under both far-from-equilibrium and near-to-equilibrium conditions, but this should be confirmed whenever possible through analysis of original experimental results.

Although it may be necessary to account for kinetic reactions in geochemical models, it is convenient to assume that such reactions are under local-equilibrium control. To assess whether local equilibrium can be assumed in geochemical models of groundwater evolution, an approach accounting for coupled fluid flow and water-rock interaction is described that can be used to estimate spatial and temporal scales of local equilibrium. The approach is demonstrated for conditions involving groundwater flow in fractures at JNC's Kamaishi *in-situ* tests site, and is also used to estimate the travel time necessary for oxidizing surface waters to migrate to the level of a HLW repository in crystalline rock.

The question of whether local equilibrium is a reasonable assumption must be addressed using an appropriate modeling approach. To be appropriate for conditions at the Kamaishi site using the modeling approach noted above, the fracture fill must closely approximate a porous medium, groundwater flow must be purely advective and diffusion of solutes across the fracture-host rock boundary must not occur. Moreover, the mineralogical and physical properties of the fracture must be homogeneous over a characteristic length that is greater than or equal to the equilibration length.

If these conditions are met, calculations suggest local equilibrium would be a valid assumption in groundwater evolution models applied to the Kamaishi site if:

- it applies to reactions involving calcite, stilbite (assuming its dissolution/ precipitation behavior is similar to that of heulandite), laumontite, albite and prehnite, but not quartz;
- Darcy flow velocities are relatively low (*e.g.*, less than about 0.1 m yr^{-1}), and
- it is based on the assumption that equilibrium corresponds to an uncertainty in the saturation index of 0.0±0.4.

If, however, actual reaction rates in the field are lower than expected, possibly because reactive surface areas are overestimated, the modeling approach may be inappropriate because it is probably unrealistic to assume that fracture mineralogy is homogeneous over fracture lengths exceeding a few meters or tens of meters.

An analytical model of redox-front migration behavior based on the stationary-state approximation to coupled fluid flow and water-rock interaction, and JNC's conceptual model of the migration of oxidizing surface waters in fractures, suggests that oxidizing solutions could travel from the surface to repository depths within 400 to 50,000 years. These travel-time estimates are relatively short compared with time periods considered in safety assessments of repository performance, which suggests that time-dependent variations in the redox environment of both the near field and geosphere may need to be accounted for in these assessments. The flow velocities and concentrations of reducing minerals assumed in JNC's conceptual model may be overly conservative, however.

7 References

Acker, J.G. and Bricker, O.P. 1992. The influence of pH on biotite dissolution and alteration kinetics at low temperature. *Geochim. Cosmochim. Acta*, 56, 3073-3092.

Amrhein, C. and Suarez, D. L. 1988. The use of a surface complexation model to describe the kinetics of ligand-promoted dissolution of anorthite. *Geochim. Cosmochim. Acta*, 52, 2785-2793.

Arthur, R. C. 1996. Estimated rates of redox-front migration in granitic rocks. SKI Report 96:35, Swedish Nuclear Power Inspectorate, Stockholm, Sweden.

Arthur, R. C., Sasamoto, H., Shibata, M., Yui, M., and Neyama, A 1999. Development of thermodynamic databases for geochemical calculations. Japan Nuclear Cycle Development Institute, Tokai-Mura, Ibaraki, Japan, Technical Report, JNC TN8400 99-079.

Bailey, A. 1974. Effects of temperature on the reaction of silicates with aqueous solutions in the low temperature range. *Proc. 2nd Int'l Symp. on Water-Rock Interaction*, Prague, 375-380.

Bales, R. C. and Morgan, J. J. 1985. Dissolution kinetics of chrysotile at pH 7 to 10. *Geochim. Cosmochim. Acta*, 49, 2281-2288.

Banfield, J. F., Ferruzzi, G. G., Casey, W. H. and Westrich, H. R. 1995. HRTEM study comparing naturally and experimentally weathered pyroxenoids. *Geochim. Cosmochim. Acta*, 59, 19-31.

Bethke, C. M. 1996. *Geochemical reaction modeling*. Oxford University Press, Oxford, U. K., 397p.

Bevan, J. and Savage, D. 1989. The effect of organic acids on the dissolution of K-feldspar under conditions relevant to burial diagenesis. *Mineral. Mag.*, 53, 415-425.

Bloom, P. R. 1983. The kinetics of gibbsite dissolution in nitric acid. *Soil Sci. Soc. Am. J.*, 47, 164-168.

Bloom, P. R. and Erich, M. S. 1987. Effect of solution composition on the rate and mechanism of gibbsite dissolution in acid solutions. *Soil Sci. Soc. Am. J.*, 51, 1131-1136.

Blum, A. E. and Stillings, L. L. 1994. Feldspar dissolution kinetics. In: *Chemical weathering rates of silicate minerals* (A. F. White and S. L. Brantley, eds.), Rev. Mineral., 31, Min. Soc. Amer., 291-351.

Brady, P. V. and Walther, J. V. 1989. Controls on silicate dissolution in neutral and basic pH solutions at 25°C. *Geochim. Cosmochim. Acta*, 53, 2823-2830.

Brady, P. V. and Carroll, S. A. 1994. Direct effects of CO_2 and temperature on silicate weathering: Possible implications for climate control. *Geochim. Cosmochim. Acta*, 58, 1853-1856.

Brantley, S. L. and Chen, Y. 1994. Chemical weathering rates of pyroxenes and amphiboles. In: *Chemical weathering rates of silicate minerals* (A. F. White and S. L. Brantley, eds.), Rev. Mineral., 31, Min. Soc. Amer., 119-172.

Bruno, J., Stumm, W., Wersin, P. and Brandberg, F. 1992. On the influence of carbonate in mineral dissolution: I. The thermodynamics and kinetics of hematite dissolution in bicarbonate solutions at T = 25°C. *Geochim. Cosmochim. Acta*, 56, 1139-1147.

Carroll, S.A. and Walther, J.V. 1990. Kaolinite dissolution at 25°, 60°, and 80°C. *Am. J. Sci.*, 290, 797-810.

Chou, L. 1985. Study of the kinetics and mechanisms of dissolution of albite at room temperature and pressure. Ph.D. dissertation. Northwestern Univ., Evanston, IL.

Chou, L. and Wollast, R. 1985. Steady-state kinetics and dissolution mechanisms of albite. *Am. J. Sci.*, 185, 963-993.

Cross, J. E., Haworth, A., Lichtner, P. C., MacKenzie, A. B., Moreno, L., Neretnieks, I., Nordstrom, D. K., Read, D., Romero, L., Scott, R. D., Sharland, S. M., and Tweed, C. J. 1991. Testing models of redox front migration and geochemistry at the Osamu Utsumi mine and Morro do Ferro analogue study sites, Poços de Caldas, Brazil. NAGRA NTB 90-30, Baden, Switzerland.

Dana, E. S. 1949. *A textbook of mineralogy, 4th ed.* John Wiley & Sons, Inc., New York, 851p.

Davis, S. N. and DeWiest, R. J. M. 1966. *Hydrogeology.* John Wiley & Sons, New York, 463p.

Delany, J. M., Puigdomenech, I. and Wolery, T. J. 1986. Precipitation kinetics option for the EQ3/6 geochemical reaction path code. UCRL-53642, Lawrence Livermore National Laboratory, Livermore, CA.

Dove, P.M. 1994. The dissolution kinetics of quartz in sodium chloride solutions at 25° to 300°C. *Am. J. Sci.*, 294, 665-712.

Dove, P.M. and Crerar, D.A. 1990. Kinetics of quartz dissolution in electrolyte solutions using a hydrothermal mixed flow reactor. *Geochim. Cosmochim. Acta*, 54, 955-969.

Drever, J. I. and Clow, D. W. 1994. Weathering rates in catchments. In: *Chemical weathering rates of silicate minerals* (A. F. White and S. L. Brantley, eds.), Rev. Mineral., 31, Min. Soc. Amer., 463-483.

Ferruzzi, G. G. 1993. The character and rates of dissolution of pyroxenes and pyroxenoids. M. S. thesis, Univ. California, Davis, CA.

Fleer, V. N. 1982. The dissolution kinetics of anorthite ($CaAl_2Si_2O_8$) and synthetic strontium feldspar ($SrAl_2Si_2O_8$) in aqueous solutions at temperatures below 100°C. Applications to the geological disposal of radioactive nuclear wastes. Ph.D. dissertation, Penn. State Univ., University Park, PA.

Furrer, G., Zysset, M. and Schindler, P. W. 1993. Weathering kinetics of montmorillonite: Investigations in batch and mixed-flow reactors. In: *Geochemistry of clay-pore fluid interactions* (D.A.C. Manning, P.T. Hughes and C. R. Hughes, eds.), Chapman & Hall, London, 243-262.

Ganor, J., Mogollón, J.L. and Lasaga, A.C. 1995. The effect of pH on kaolinite dissolution rates and on activation energy. *Geochim. Cosmochim. Acta,* 59(6), 1037-1052.

Gautier, J.-M., Oelkers, E. H. and Schott, J. 1994. Experimental study of K-feldspar dissolution rates as a function of chemical affinity at 150°C and pH 9. *Geochim. Cosmochim. Acta*, 58, 4549-4560.

Gislason, S. R., Heaney, P. J., Oelkers, E. H. and Schott, J. 1997. Kinetic and thermodynamic properties of moganite, a novel silica polymorph. *Geochim. Cosmochim. Acta*, 61(6), 1193-1204.

Grandstaff, D. E. 1977. Some kinetics of bronzite orthopyroxene dissolution. *Geochim. Cosmochim. Acta*, 41, 1097-1103.

Helgeson, H. C. 1968. Evaluation of irreversible reactions in geochemical processes involving minerals and aqueous solutions –I. Thermodynamic relations. *Geochim. Cosmochim. Acta,* 32, 853-877.

Helgeson, H. C., Murphy, W. M. and Aagaard, P. 1984. Thermodynamic and kinetic constraints on reaction rates among minerals and aqueous solution. II. Rate constants, effective surface area, and the hydrolysis of feldspar. *Geochim. Cosmochim. Acta*, 48, 2405-2432.

Hellmann, R. 1994. The albite-water system: Part I. The kinetics of dissolution as a function of pH at 100, 200 and 300°C. *Geochim. Cosmochim. Acta*, 58, 595-611.

Heydemann, A. 1966. Über die chemische verwitterung von tonmineralen (experimentelle untersuchungen). *Geochim. Cosmochim. Acta*, 30, 995-1035.

Hill, G. G., Jr. 1977. *An introduction to chemical engineering kinetics and reactor design.* John Wiley & Sons, New York, 594p.

Holdren, G. R. and Speyer, P. M. 1985. pH dependent change in the rates and stoichiometry of dissolution of an alkali feldspar at room temperature. *Am. J. Sci.*, 285, 994-1026.

Holdren, G. R. and Speyer, P. M. 1987. Reaction rate-surface area relationships during the early stages of weathering. II. Data on eight additional feldspars. *Geochim. Cosmochim. Acta*, 51, 2311-2318.

Hume, I. A. and Rimstidt, J. D. 1992. The biodurability of chrysotile asbestos. *Am. Mineral.*, 77, 1125-1128.

Johnson, J. W., Oelkers, E. H., and Helgeson, H. C. 1992. SUPCRT92: A software package for calculating the standard molal thermodynamic properties of minerals, gases, aqueous species, and reactions from 1 to 5000 bars and 0° to 100°C. *Computers and Geosciences*, 18, 899-947.

Kalinowski, B.E. and Schweda, P. 1996. Kinetics of muscovite, phlogopite, and biotite dissolution and alteration at pH 1 -4, room temperature. *Geochim. Cosmochim. Acta*, 60(3), 367-385.

Kline, W. E. and Fogler, H. S. 1981. Dissolution kinetics: The nature of the particle attack of layered silicate in HF. *Chem. Eng. Sci.*, 36, 871-884.

Knapp, R. B. 1989. Spatial and temporal scales of local equilibrium in dynamic fluid-rock systems. *Geochim. Cosmochim. Acta*, 53, 1955-1964.

Knauss, K. and Wolery, T. J. 1986. Dependence of albite dissolution kinetics on pH and time at 25°C and 70°C. *Geochim. Cosmochim. Acta*, 50, 2481-2497.

Knauss, K. and Wolery, T. J. 1989. Muscovite dissolution kinetics as a function of pH and time at 70°C. *Geochim. Cosmochim. Acta*, 53, 1493-1502.

Knauss, K., Nguyen, S.N. and Weed, H.C. 1993. Diopside dissolution kinetics as a function of pH, CO_2, temperature, and time. *Geochim. Cosmochim. Acta*, 57, 285-294.

Kuwahara, Y. and Aoki, Y. 1995. Dissolution process of phlogopite in acid solutions. *Clays Clay Minerals*, 43, 39-50.

Lichtner, P. C. 1985. Continuum model for simultaneous chemical reactions and mass transport in hydrothermal systems. *Geochim. Cosmochim. Acta*, 49, 779 - 800.

Lichtner, P. C. 1988. The quasi-stationary state approximation to coupled mass transport and fluid-rock interaction in a porous medium. *Geochim. Cosmochim. Acta.*, 52, 143 - 165.

Lichtner, P. C. and Waber, N. 1992. Redox front geochemistry and weathering: Theory with application to the Osamu Utsumi uranium mine, Poços de Caldas, Brazil. *Jour. Geochem. Explor.*, 45 (1/3), 521-564.

Lin, F.-C. and Clemency, C. V. 1981a. Dissolution kinetics of phlogopite. 1. Closed system. *Clays Clay Minerals*, 29, 101-106.

Lin, F.-C. and Clemency, C. V. 1981b. The kinetics of dissolution of muscovites at 25°C and 1 atm CO_2 partial pressure. *Geochim. Cosmochim. Acta*, 45, 571-576.

Lin, F.-C. and Clemency, C. V. 1981c. The dissolution kinetics of brucite, antigorite, talc and phlogopite at room temperature and pressure. *Am. Mineral.*, 66, 801-806.

MacKenzie, A. B., Scott, R. D., Linsalata, P., Miekelley, N., Osmond, J. K., and Curtis, D. B. 1991. Natural radionuclide and stable element studies of rock samples from the Osamu Utsumi mine and Morro do Ferro analogue study sites, Poços de Caldas, Brazil. NAGRA NTB 90-25.

May, H. M., Acker, J. G., Smyth, J. R., Bricker, O. P. and Dyar, M. D. 1995. Aqueous dissolution of low-iron chlorite in dilute acid solutions at 25°C. *Clay Minerals Soc. Prog. Abstr.*, 32, 88.

Mogollon, J. L., Perez, D. A., Lo Monaco, S., Ganor, J. and Lasaga, A. C. 1994. The effect of pH, $HClO_4$, HNO_3 and ΔG_r on the dissolution rate of natural gibbsite using column experiments. *Mineral. Mag.*, 58A, 619-620.

Murphy, W.M. and Helgeson, H.C. 1989. Thermodynamic and kinetic constraints on reaction rates among minerals and aqueous solutions. IV. Retrieval of rate constants and activation parameters for the hydrolysis of pyroxene, wollastonite, olivine, andalusite, quartz, and nepheline. *Am. J. Sci.*, 289, 17-101.

Murphy W.M., Pabalan R.T., Prikryl J.S. and Goulet C.J. 1996. Reaction kinetics and thermodynamics of aqueous dissolution and growth of analcime and Na-clinoptilolite at 25°C. *Am. J. Sci., 296*, 128-186.

Nagy, K. L. 1994. Dissolution and precipitation kinetics of sheet silicates. In: *Chemical weathering rates of silicate minerals* (A. F. White and S. L. Brantley, eds.), Rev. Mineral., 31, Min. Soc. Amer., 173-233.

Nagy, K.L. and Lasaga, A.C. 1992. Dissolution and precipitation kinetics of gibbsite at 80°C and pH 3: The dependence on solution saturation state. *Geochim. Cosmochim. Acta*, 56, 3093-3111.

Nagy, K.L., Blum, A.E. and Lasaga, A.C. 1991. Dissolution and precipitation kinetics of kaolinite at 80°C and pH 3: The dependence on solution saturation state. *Am. J. Sci.*, 291, 649-686.

Nickel, E. 1973. Experimental dissolution of light and heavy minerals in comparison with weathering and intrastratal solution. *Contrib. Sedimentology*, 1, 1-68.

Oelkers, E.H. and Schott, J. 1995. Experimental study of anorthite dissolution and the relative mechanism of feldspar hydrolysis. *Geochim. Cosmochim. Acta*, 59(24), 5039-5053.

Oelkers, E. H., Schott, J. and Devidal, J. L. 1994. The effect of aluminum, pH and chemical affinity on the rates of aluminosilicate dissolution reactions. *Geochim. Cosmochim. Acta*, 58, 2011-2024.

Ortoleva, P., Auchmuty, G., Chadam, J., Hettmer, J. Merino, E., Moore, C. H. and Ripley, E. 1986. Redox front propagation and banding modalities. *Physica*, 19D, 334 - 354.

Osawa, H., Sasamoto, H., Nohara, T., Oka, K. and Yoshida, H. 1995. Development of a conceptual flow-path model of nuclide migration in crystalline rock – A case study at the Kamaishi in-situ test site, Japan. In. *Scientific basis for nuclear waste management XVIII* (T. Murakami and R. C. Ewing, eds.), Mat. Res. Soc., Pittsburgh, PA, 1267-1273.

Oxburgh, R., Drever, J. I. and Sun, Y. T. 1994. Mechanism of plagioclase dissolution in acid solution at 25C. *Geochim. Cosmochim. Acta*, 58, 661-669.

Paces, T. 1972. Chemical characteristics and equilibration between ground water and granitic rock. *Geochim. Cosmochim. Acta*, 36, 217 - 240.

Paces, T. 1983. Rate constants of dissolution derived from the measurements of mass balance in hydrological catchments. *Geochim. Cosmochim. Acta*, 47, 1855 - 1863.

Packter, A. and Dhillon, H. S. 1973. The kinetics and mechanism of the heterogeneous reactions of crystallized gibbsite powders with aqueous sodium hydroxide solutions: Kinetics and mechanism. *J. Phys. Chem.*, 77, 2942-2947.

Packter, A. and Dhillon, H. S. 1974. Studies on recrystallized aluminum hydroxide precipitates: Kinetics and mechanism of dissolution by sodium hydroxide solutions. *Coll. Polymer Sci.*, 252, 249-256.

Plummer, L. N., Wigley, T. M. L., and Parkhurst, D. L. 1978. The kinetics of calcite dissolution in CO_2-water systems at 5° and 60°C and 0.0 to 1.0 atm. CO_2. *Am. J. Sci.*, 278, 179-216.

Posey-Dowty, J., Crerar, D., Hellmann, R. and Chang, C. D. 1986. Kinetics of mineral-water reactions: theory, design and application of circulating hydrothermal equipment. *Am. Mineral.*, 71, 85-94.

Ragnarsdóttir, K.V. 1993. Dissolution kinetics of heulandite at pH 2 - 12 and 25C. *Geochim. Cosmochim. Acta,* 57, 2439-2449.

Reddy, M. M., Plummer, L. N. and Busenberg, E. 1981. Crystal growth of calcite from calcium bicarbonate solutions at constant P_{CO2} and 25°C: A test of a calcite dissolution model. *Geochim. Cosmochim. Acta,* 45, 1281-1289.

Rhén, I., Svensson, U., Andersson, J.-K., Andersson, P., Eriksson, C.-O., Gustafsson, E., Ittner, T. and Nordqvist, R. 1992. Äspö hard rock laboratory. Evaluation of the combined long-term pumping and tracer test (LPT2) in borehole KAS06. SKB TR 92-32, Swedish Nuclear Fuel and Waste Management Co., Stockholm, Sweden.

Rickard, D. 1995. Kinetics of FeS precipitation: Part I. Competing reaction mechanisms. *Geochim. Cosmochim. Acta,* 59(21), 4367-4379.

Rimstidt, J. D. 1997. Quartz solubility at low temperatures. *Geochim. Cosmochim. Acta,* 61(3), 2553-2558.

Rimstidt, J. D. and Barnes, H.L. 1980. The kinetics of silica-water reactions. *Geochim. Cosmochim. Acta,* 44(11), 1683-1699.

Rimstidt, J. D. and Dove, P. M. 1986. Mineral/solution reaction rates in a mixed flow reactor: wollastonite hydrolysis. *Geochim. Cosmochim. Acta,* 50, 2509-2516.

Romero, L., Moreno, L., and Neretnieks, I. 1990. Modeling of the movement of the redox front in the uranium mine in Poços de Caldas, Brazil. SKB TR 90-39, Swedish Nuclear Fuel and Waste Management Co., Stockholm, Sweden.

Ross, G. J. 1967. Kinetics of acid dissolution of an orthochlorite mineral. *Can. J. Chem.,* 45, 3031-3034.

Sanemasa, I and Katsura, T. 1973. The dissolution of $CaMg(SiO_3)_2$ in acid solutions. *Bull. Chem. Soc. Japan,* 46, 3416-3422.

Sasamoto, H., Kitayama, M., Sato, M., Yoshida, H., Ota, K., Nohara, T. and Takeda, S. 1993. Fracture mapping in the E.L. 250 m drift in the Kamaishi Mine. PNC Technical Report KTR 93-02, TN7410 93-032 (in Japanese with English abstract).

Sasamoto, H., Yui, M. and Arthur, R. C. 1999a. Status of geochemical modeling of groundwater evolution at the Tono *in-situ* tests site, Japan. Japan Nuclear Cycle Development Institute, Tokai-Mura, Ibaraki, Japan, Technical Report, JNC TN8400 99-074.

Sasamoto, H., Yui, M. and Arthur, R. C. 1999b. Hydrochemical investigation and status of geochemical modeling of groundwater evolution at the Kamaishi *in-situ* tests site,

Japan. Japan Nuclear Cycle Development Institute, Tokai-Mura, Ibaraki, Japan, Technical Report, JNC TN8400-033.

Sasamoto, H., Yui, M. and Arthur, R. C. 1999c. Modeling studies of saline type groundwater evolution – A test case for Mobara groundwater chemistry, Japan. Japan Nuclear Cycle Development Institute, Tokai-Mura, Ibaraki, Japan, Technical Report (in preparation).

Savage, D., Cave, M.R., Haigh, D., Mildowski, A.E., and Young, M. E. 1993. The reaction kinetics of laumontite under hydrothermal conditions. *Eur. J. Mineral.*, 5, 523-535.

Savage, D., Lemke, K., Sasamoto, H., Shibata, M., Arthur, R. C. and Yui, M. 1999. Compilation of thermodynamic data for hyperalkaline systems. Japan. Japan Nuclear Cycle Development Institute, Tokai-Mura, Ibaraki, Japan, Technical Report (in preparation).

Schott, J. and Berner, R. A. 1983. X-ray photoelectron studies of the mechanism of iron silicate dissolution during weathering. *Geochim. Cosmochim. Acta*, 47, 2233-2240.

Schott, J. and Berner, R. A. 1985. Dissolution mechanisms of pyroxenes and olivines during weathering. In: *The chemistry of weathering* (J. I. Drever, ed.), NATO ASI Series C; Mathematical and Physical Sciences, 149, 35-53.

Schott, J. and Petit, J. C. 1987. New evidence for the mechanisms of dissolution of silicate minerals. In: *Aquatic surface chemistry: Chemical processes at the particle-water interface* (W. Stumm, ed.), Swiss Fed. Inst. Technol., Zurich, Switzerland, 293-315.

Schott, J., Berner, R. A. and Sjoberg, E. L. 1981. Mechanism of pyroxene and amphibole weathering – I. Experimental studies of iron-free minerals. *Geochim. Cosmochim. Acta*, 45, 2123-2135.

Schweda, P. 1990. Kinetics and mechanisms of akali feldspar dissolution at low temperatures. Ph.D. dissertation, Stockholm Univ., Stockholm, Sweden.

Siegel, D. I. and Pfannkuch, H. O. 1984. Silicate mineral dissolution at pH 4 and near standard temperature and pressure. *Geochim. Cosmochim. Acta*, 48, 197-201.

Sjöberg, L. 1989. Kinetics and non-stoichiometry of labradorite dissolution. In: *Proc. 6th Int'l Symp. on Water-Rock Interaction* (D. L. Miles, ed). A.A. Balkema, Rotterdam, 639-642.

Stumm, W., Wehrli, B. and Wieland, E. 1987. Surface complexation and its impact on geochemical kinetics. *Croatica Chemica Acta*, 60, 429-456.

Sverdrup, H.U. 1990. *The kinetics of base cation release due to chemical weathering.* Lund Univ. Press, Lund, Sweden, 246p.

Thomassin, J. H., Goni, J., Baillif, P., Touray, J. C. and Jaurand, M. C. 1977. An XPS study of the dissolution kinetics of chrysotile in 0.1 N oxalic acid at different temperatures. *Phys. Chem. Minerals*, 1, 385-398.

Thompson, J. B., Jr. 1959. Local equilibrium in metasomatic processes. In. *Researches in geochemistry* (P. H. Abelson, ed.). Wiley and Sons, New York, 427-457.

Thompson, A. F. B. and Jackson, K. J. 1996. Reactive transport in heterogeneous systems: An overview. In. *Reactive transport in porous media* (P. C. Lichtner, C. I. Steefel and E. H. Oelkers, eds.). Rev. Mineral., 34, Min. Soc. Am., Wash., D. C., 269-310.

Velbel, M. A. 1985. Geochemical mass balances and weathering rates in forested watersheds of the southern Blue Ridge. *Am. J. Sci.*, 285, 904-930.

Vermilyea, D. A. 1969. The dissolution of MgO and $Mg(OH)_2$ in aqueous solutions. *J. Electrochem. Soc.*, 116, 1179-1183.

Weast, R. C. 1979. *CRC handbook of chemistry and physics, 60th ed.* CRC Press, Inc., Boca Raton, Fl.

White, A. F. and Peterson, M. L. 1990. Role of reactive-surface-area characterization in geochemical kinetic models. In *Chemical modeling of aqueous systems II*, (D. C. Melchior and R. L. Bassett, eds.), ACS Ser. 416, American Chemical Society, Washington, D.C., 461-475.

White, A.F., Peterson, M.L. and Hochella, M.F., Jr. 1994. Electrochemistry and dissolution kinetics of magnetite and ilmenite. *Geochim. Cosmochim. Acta*, 58(8), 1859-1875.

Wieland, E. and Stumm, W. 1992. Dissolution kinetics of kaolinite in acidic solutions at 25C. *Geochim. Cosmochim. Acta*, 56, 3339-3355.

Wikberg, P., Gustafson, G. Rhén, I. and Stanfors, R. 1991. Äspö hard rock laboratory. Evaluation and conceptual modeling based on the pre-investigations. SKB TR 91-22, Swedish Nuclear Fuel and Waste Management Co., Stockholm, Sweden.

Williamson, M.A. and Rimstidt J.D. 1994. The kinetics and electrochemical rate-determining step of aqueous pyrite oxidation. *Geochim. Cosmochim. Acta,* 58(24), 5443-5454.

Wogelius, R. A. and Walther, J. V. 1992. Olivine dissolution kinetics at near-surface conditions. *Chem. Geol.*, 97, 101-112.

Wolery, T. J. 1983. EQ3NR, a computer program for geochemical aqueous speciation-solubility calculations: user's guide and documentation. Lawrence Livermore National Laboratory Report UCRL-53414, Livermore, CA.

Wolery, T. J. 1992. EQ3/6, a software package for geochemical modeling of aqueous systems: package overview and installation guide (Version 7.0). Lawrence Livermore National Laboratory Report UCRL-MA-110662 PT I, Livermore, CA.

Wollast, R. and Chou, L. 1992. Surface reactions during the early stages of weathering of albite. *Geochim. Cosmochim. Acta*, 56, 3113-3122.

Xie, Z. 1994. Surface properties of silicates, their stability and dissolution kinetics. Ph.D. dissertation, Northwestern Univ., Evanston, IL.

Yui, M., Sasamoto, H. and Arthur, R. C. 1999. Groundwater evolution modeling for the 2nd progress (PA) report. Japan Nuclear Cycle Development Institute, Tokai-Mura, Ibaraki, Japan, Technical Report, JNC TN8400-030.

Zhang, H. 1990. Factors determining the rate and stoichiometry of hornblende dissolution. Ph.D. dissertation. Univ. Minnesota, Minneapolis, MN.

Zhong, S. and Mucci, A. 1993. Calcite precipitation in seawater using a constant addition technique: A new overall reaction kinetic expression. *Geochim. Cosmochim. Acta*, 57, 1409-1417.

Zuddas, P. and Mucci, A. 1994. Kinetics of calcite precipitation from seawater: I. A classical chemical kinetics description for strong electrolyte solutions. *Geochim. Cosmochim. Acta*, 58(20), 4353-4362.

Appendix: Analytical Model of Redox-Front Velocities

The following derivation is based on that described by Lichtner (1985, 1988), who adopted a continuum representation of mass transport in a porous medium involving a multicomponent system of reacting minerals and fluid. Homogeneous reactions among aqueous species are assumed to be sufficiently fast to sustain equilibrium. Heterogeneous reactions among minerals and the aqueous phase are, however, described in terms of kinetic rate laws, for which local equilibrium is a limiting case.

Lichtner (1985) represents chemical reactions in such systems for primary aqueous species, j, and irreversibly reacting minerals, r, by the following set of $N + M$ coupled, non-linear partial differential equations:

$$\frac{\partial}{\partial t}(\phi\psi_j)+\nabla\bullet\Omega_j=-\sum_{r=1}^{M}\nu_{j,r}\frac{\partial\Xi_r}{\partial t}(j=1,...,N), \text{ and} \tag{A.1}$$

$$\frac{\partial}{\partial t}(\phi_r\bar{V}_r^{-1})=\frac{\partial\Xi_r}{\partial t}(r=1,...,M). \tag{A.2}$$

Eqns. (A.1) and (A.2) refer to aqueous species and minerals, respectively. The term $\partial\Xi_r/\partial t$ denotes the reaction rate for dissolution of the r-th mineral and Ω_j represents the generalized flux (other symbols are as defined in Section 5.3). Although Lichtner (1985) defines the flux term rigorously, this is unnecessary for the present discussion because the relations to be derived are relevant only for the case of advection-dominated systems.

Lichtner (1988) combines Eqns. (A.1) and (A.2) to obtain the transient mass conservation equations for a single spatial dimension:

$$\frac{\partial}{\partial t}\left(\phi\psi_j+\sum_{r=1}^{M}\left(\frac{\nu_{j,r}}{\bar{V}_r}\right)\phi_r\right)-\phi D\frac{\partial^2\psi_j}{\partial^2 x}+v\frac{\partial\psi_j}{\partial x}=0, \tag{A.3}$$

where D refers to the diffusion coefficient matrix consisting of equal and constant elements for primary and secondary species containing j. The travelling wave approximation (Ortoleva *et al.*, 1986) is then used to derive an expression for the velocity of a reaction front appropriate for this system. The approximation is used to specify a coordinate system at rest with respect to a Lagrangian reference mass of solution moving with the front. It is assumed that one or more reaction fronts may exist, with the front of interest located at position $l(t)$, propagating with velocity $v_f = dl/dt$, and that other possible fronts in the system are sufficiently well separated so as not to overlap and interfere with each other.

The approximation assumes that near a reaction front the solution to the mass-transport equations can be represented in the form of a travelling wave, given by:

$\psi_j(x,t) = \psi_j(x - l(t))$, and

$\phi_r(x,t) = \phi_r(x - l(t))$,

for the generalized solute concentration and mineral volume fraction, respectively. Equation (A.3) is transformed to:

$$\frac{d}{dx'}\left\{-\phi D\frac{d\psi_j}{dx'} + v\psi_j - v_f\left(\phi\psi_j + \sum_{r=1}^{M}\frac{\nu_{j,r}}{\overline{V}_r}\phi_r\right)\right\} = 0 \qquad \text{(A.4)}$$

using the approximations for $\psi_j(x, t)$ and $\phi_r(x, t)$ with respect to the coordinate x', defined by $x' = x - l(t)$

From Eqn. (A.4) it follows that:

$$-\phi D\frac{d\psi_j}{dx'} + v\psi_j - v_f\left(\phi\psi_j + \sum_{r=1}^{M}\frac{\nu_{j,r}}{\overline{V}_r}\phi_r\right) = \text{constant.} \qquad \text{(A.5)}$$

Evaluating the left-hand side of this equation at two distinct points, one immediately upstream of the reaction front and the other immediately downstream, for the case of pure advective transport (*i.e.*, when the first term is negligible compared to the second term), yields:

$$v_f = \frac{v}{\phi(1 + L_j)}, \qquad \text{(A.6)}$$

where the quantity $(1 + L_j)$ represents a retardation factor, with

$$L_j = \frac{\sum_{r=1}^{M}\left(\frac{\nu_{j,r}}{\overline{V}_r}\right)\{\phi_r\}}{\phi\{\psi_j\}}, \qquad \text{(A.7)}$$

and where the brackets, { }, refer to the difference in the enclosed quantity at the two chosen points.

Lichtner (1988) furthermore proves that the traveling wave approximation is invalid when diffusional transport is important, and, therefore, that Eqn. (5.3.1.3) is also invalid under such conditions. It is also shown that Eqn. (A.6) is formally similar to the result obtained in the limit of local equilibrium, in which case the brackets are taken to represent the "jump" in ψ_j and ϕ_r at local equilibrium on either side of the front.

Application of Eqn. (5.3.1.3) for the case of reaction fronts in crystalline rocks is appropriate if fluid-flow behavior approximates that which would occur in a porous medium. This is a good approximation for two limiting cases:

- flow occurs, with negligible matrix diffusion, in individual fractures that are partially filled with alteration minerals, and

- flow occurs in fracture zones, the hydrogeologic properties of which approximate an equivalent porous medium.

Both these cases are realistic for crystalline rocks. It is possible that matrix diffusion could be an important mass-transport mechanism in these rocks, but this is ignored in the present study to maintain conservatism in the calculations. The analytical model may require modification if applied to situations in which flow occurs in individual "fresh" fractures containing little or no fracture-fill minerals